

NUCLEOSYNTHESIS AND MIXING ON THE ASYMPTOTIC  
GIANT BRANCH.  
III. PREDICTED AND OBSERVED *s*-PROCESS  
ABUNDANCES

Maurizio Busso<sup>1</sup>, Roberto Gallino<sup>2</sup>, David L. Lambert<sup>3</sup>,  
Claudia Travaglio<sup>4</sup>, and Verne V. Smith<sup>5</sup>

1. Osservatorio Astronomico di Torino, Torino, I-10025 Pino Torinese, Italy,  
busso@to.astro.it
2. Dipartimento di Fisica Generale, Università di Torino, Via P. Giuria 1, I-10125 Torino,  
Italy, gallino@ph.unito.it
3. Department of Astronomy, University of Texas at Austin, TX 78741, USA,  
dll@astro.as.utexas.edu
4. Max-Planck Institut für Astronomie, Königstuhl 17, D-69117 Heidelberg, Germany,  
claudia@mpia-hd.mpg.de
5. Department of Astronomy, University of Texas at El Paso, TX 79968, USA,  
verne@barium.physics.utep.edu

## ABSTRACT

We present the results of *s*-process nucleosynthesis calculations for Asymptotic Giant Branch (AGB) stars of different metallicities and different initial stellar masses (1.5 and 3  $M_{\odot}$ ) and comparisons of them with observational constraints from high resolution spectroscopy of evolved stars over a wide metallicity range. The computations were based on previously published stellar evolutionary models that account for the third dredge up phenomenon occurring late on the AGB. Neutron production is driven by the  $^{13}\text{C}(\alpha, n)^{16}\text{O}$  reaction during the interpulse periods in a tiny layer in radiative equilibrium at the top of the He- and C-rich shell. The neutron source  $^{13}\text{C}$  is manufactured locally by proton captures on the abundant  $^{12}\text{C}$ ; a few protons are assumed to penetrate from the convective envelope into the radiative layer at any third dredge up episode, when a chemical discontinuity is established between the convective envelope and the He- and C-rich zone. A weaker neutron release is also guaranteed by the marginal activation of the reaction  $^{22}\text{Ne}(\alpha, n)^{25}\text{Mg}$  during the convective thermal pulses. Owing to the lack of a consistent model for  $^{13}\text{C}$  formation, the abundance of  $^{13}\text{C}$  burnt per cycle is allowed to vary as a free parameter over a wide interval (a factor of 50). The *s*-enriched material is subsequently mixed with the envelope by the third dredge up, and the envelope composition is computed after each thermal pulse. We follow the changes in the photospheric abundance of the Ba-peak elements (heavy *s*, or ‘hs’) and that of the Zr-peak ones (light *s*, or ‘ls’), whose logarithmic ratio [hs/ls] has often been adopted as an indicator of the *s*-process efficiency (e.g. of the neutron exposure). Our model predictions for this parameter show a complex trend versus metallicity. Especially noteworthy is the prediction that the flow along the *s* path at low metallicities drains the Zr-peak and Ba-peak and builds an excess at the doubly-magic  $^{208}\text{Pb}$ , at the termination of the *s* path. We then discuss the effects on the models of variations in the crucial parameters of the  $^{13}\text{C}$  pocket, finding that they are not critical for interpreting the results.

The theoretical predictions are compared with published abundances of *s* elements for AGB giants of classes MS, S, SC, post-AGB supergiants, and for various classes of binary stars, which supposedly derive their composition by mass transfer from an AGB companion. This is done for objects belonging both to the Galactic disk and to the halo. The observations in general confirm the complex dependence of neutron captures on metallicity. They suggest that a moderate spread exists in the abundance of  $^{13}\text{C}$  that is burnt in different stars. Although additional observations are needed, it seems that a good understanding has been achieved of *s*-process operation in AGB stars. Finally, the detailed

abundance distribution including the light elements (CNO) of a few *s*-enriched stars at different metallicity are examined and satisfactorily reproduced by model envelope compositions.

*Subject headings:* stars: AGB – stars: evolution – stars: low mass – nucleosynthesis

## 1. Introduction

In this paper we present an interpretation of the observed *s*-element abundances in evolved red giants in the light of current models for the nucleosynthesis occurring in low mass stars. The red giants studied here are primarily those powered by hydrogen and helium burning in two shells located above a degenerate C-O core and are called Asymptotic Giant Branch (AGB) stars, see e.g. Iben & Renzini (1983). Late on the AGB, they undergo recurrent thermal instabilities of the He-shell (thermal pulses, TP), where partial He burning occurs convectively over short periods of time, sweeping the whole region that lies between the H and the He shells (hereafter, the He intershell). The stars undergoing such processes are semiregular or Mira variables showing the short-lived Tc in their spectra (Merrill 1952). They belong to the spectral types MS, S, SC, or C(N) and are called *intrinsic* TP-AGB stars (Lambert 1985; Smith & Lambert 1990, hereafter SL90; Plez, Smith, & Lambert 1993). Strong and variable stellar winds, with mass loss rates  $dM/dt$  from  $10^{-7}$  up to  $10^{-5} M_{\odot}/\text{yr}$ , progressively reduce their envelopes, leaving behind a degenerate C-O core, which will eventually become a white dwarf. During the TP-AGB phase, material from the He intershell, enriched in  $^{12}\text{C}$ ,  $^{22}\text{Ne}$ , and *s*-process elements, appears at the surface, thanks to repeated downward extensions of the envelope convection (third dredge up, TDU). In other cases, the star that was the site of the *s*-element synthesis appears to have left the TP-AGB phase, ejecting most of its envelope and exposing the hot layers immediately above the H shell. Such a star appears as a post-AGB carbon-rich and *s*-element-rich supergiant of classes A, F, or G (Van Winckel & Reyniers 2000).

Further constraints on neutron-capture nucleosynthesis in the Galaxy come from binary systems, in which the more massive component, while on the TP-AGB phase, has transferred part of its envelope onto a lower mass companion, now seen to be enriched in *s*-elements. It is therefore this companion (*extrinsic* AGB) that becomes the object of our study (see Jorissen & Mayor 1988; Han et al. 1995; Jorissen et al. 1998 for a treatment of mass transfer and Ba-star masses, and Smith 1984, Luck & Bond 1991a,b, Luck, Bond, & Lambert 1990 for details on the resulting abundances). In this group of stars we find the classical Ba II

giants, and other sources in which the secondary component has in its turn evolved to the early AGB phases, so that it can be distinguished from ‘normal’ MS, S, SC and C(N) stars only by the absence of Tc. The group of extrinsic AGBs also contains several classes of CH-strong dwarfs, subgiants and giants at various metallicities. These are low luminosity stars with *s*-process enrichments that are most probably not spectroscopic binaries, e.g., the N-rich subdwarf HD 25329 (Beveridge & Sneden 1994), and HD 23439A and B (Tomkin & Lambert 1999). In these cases, it is presumed that their natal clouds were contaminated by ejecta from AGB stars. This is e.g. the case of the *s* enrichment in red giants belonging to the globular cluster  $\omega$  Cen (Smith et al. 2000).

As far as nucleosynthesis is concerned, current studies ascribe neutron captures to the activation of the reactions  $^{13}\text{C}(\alpha, n)^{16}\text{O}$  and  $^{22}\text{Ne}(\alpha, n)^{25}\text{Mg}$  (Iben & Renzini 1982; Hollowell & Iben 1988; Gallino et al. 1988; Käppeler et al. 1990; Busso, Gallino, & Wasserburg 1999, hereafter BGW99). The same reactions may also affect the nucleosynthesis of lighter nuclei, like fluorine, sodium, and the unstable  $^{26}\text{Al}$  (Mowlavi & Meynet, 2000; Goriely & Mowlavi 2000; Mowlavi 1999).

The principal goal of this paper is to verify the ability of current forms of AGB models to account for the observed abundance distributions in evolved stars. In § 2 we discuss the general features of our models and the choices made for the parameterization of the neutron source  $^{13}\text{C}$ . We also comment on the major effects on *s*-process nucleosynthesis introduced by varying the initial metallicity. A comparison of observed heavy element abundances of intrinsic and extrinsic *s*-enriched stars with model predictions follows in § 3. Detailed fits to the observed compositions including the light elements of three selected stars are sketched in § 4. Finally, in § 5 we summarize the main conclusions that can be drawn from such an analysis.

## 2. The Adopted Models for Stellar Evolution and Nucleosynthesis

### 2.1. Indices of *s*-processing

Abundance analyses of stars enriched by *s*-processing may often provide quantitative information for only a few neutron rich elements. This has led to simple characterizations of the overabundances. Following Luck & Bond (1991a,b), it is common to monitor the *s*-process efficiency through the relative abundances of the *s* elements at the Ba-peak (collectively indicated as ‘heavy *s*’, or ‘hs’) with respect to those at the Zr-peak (indicated as ‘light *s*’ or ‘ls’). Indeed, those nuclei are placed at neutron magic numbers  $N = 82$  and 50, are mainly of *s*-process origin and act as bottlenecks for the *s*-process path because of their

low neutron capture cross sections. Consequently, for relatively low  $s$ -process efficiencies, the neutron flux mainly feeds the nuclei at the Zr-peak, while for higher exposures the Ba-peak species are favored (see § 3.1 for a deeper analysis). The average logarithmic ratio normalized to solar,  $[\text{hs}/\text{ls}]$ , defined as  $[\text{hs}/\text{ls}] = \log (\text{hs}/\text{ls})_* - \log (\text{hs}/\text{ls})_\odot$ , has been extensively used as a measure of the neutron capture efficiency in building up the heavy  $s$  elements and proved useful for the interpretation of the Galactic disk stars (Busso et al. 1992, 1995, hereafter Paper I and Paper II, respectively). The choice of the specific elements to consider in the average ‘hs’ and ‘ls’ abundances varies from author to author and depends on the quality of the spectra available. The definition adopted by Luck & Bond (1991a,b) included Sr, Y, Zr in the ‘ls’ group and Ba, La, Nd, Sm in the ‘hs’ one. In presenting the model results we instead consider Y and Zr as ‘ls’. We generally exclude Sr, despite the fact that it is mainly of  $s$ -process origin, because it has been measured precisely only in a minority of the sample stars. For the ‘hs’ group, we include La and Nd, which are present with several lines in most sample stars. The results would not be significantly changed if we adopted the same choice as Luck & Bond (1991a,b). Whenever possible, we follow the same rules in selecting the observations. There are however cases in which this is not possible. One is represented by the star CS 22898-027 (McWilliam et al. 1995) where ‘ls’ can be defined only through Sr (Y and Zr were not measured). For ‘hs’ the situation is more complex. There are cases in which only one element of the couple La, Nd was measured, in other cases only estimates of the Ba abundance exist, etc. The stars affected by such problems are commented explicitly later, in order to make clear which choices were made (see discussion of Table 2). These limitations increase slightly the uncertainties in the constraints.

In addition, the degree of  $s$ -process enrichment is of interest. We consider the logarithmic ratios, normalized to solar,  $[\text{ls}/\text{Fe}]$  and  $[\text{hs}/\text{Fe}]$  as measures of the enrichment. For the intrinsic stars, both indices increase with the number of TDUs but the ratio  $[\text{hs}/\text{ls}]$  after a relatively few TDUs approaches an asymptotic value. In the case of the extrinsic stars, the  $[\text{ls}/\text{Fe}]$  and  $[\text{hs}/\text{Fe}]$  are dependent on the values of these indices in the AGB envelope during mass transfer and on the degree of dilution occurring in the extrinsic star on receipt of the mass or subsequently.

For a few stars, a quite extensive array of heavy elements have been measured, and, in these cases, theoretical models may be tested for their ability to reproduce the suite of elemental abundances, a finer test than that possible using indices ‘ls’ and ‘hs’.

## 2.2. General Characteristics of $s$ Processing in AGB Stars

As mentioned, the main neutron source allowing  $s$ -processing to take place in AGB stars is the reaction  $^{13}\text{C}(\alpha, n)^{16}\text{O}$ . Its activation requires the penetration of a small amount of protons from the envelope into the He intershell (i.e. the region between the H and He shells), most likely occurring during the post-flash luminosity dip, when the H shell is extinguished and TDU can occur (Iben & Renzini 1983). Studies on the required mixing mechanisms have made use of diffusive or hydrodynamical simulations (Iben & Renzini 1982; Hollowell & Iben 1988; Herwig et al. 1997; Herwig 2000; Cristallo et al. 2001). They are still a matter of debate, though a consensus is emerging that partial mixing must indeed occur. At least in some cases it may also be affected by rotational shears (Langer et al. 1999), but a self-consistent model is still not possible in stellar codes. Due to these uncertainties, the amount of  $^{13}\text{C}$  that forms in a *pocket* at the top of the He intershell and its profile in mass must be represented by free parameters. Introducing a range of  $^{13}\text{C}$  abundances at a given metallicity proved to be effective for several purposes (see, e.g., Gallino et al. 1998, hereafter G98; Travaglio et al. 1999, hereafter T99, Goriely & Mowlavi, 2000).

The alternative to the  $^{13}\text{C}$  neutron source is the  $^{22}\text{Ne}(\alpha, n)^{25}\text{Mg}$  reaction, which is triggered when the temperature  $T$  exceeds  $3 \times 10^8$  K, but this reaction does not play a dominant role in AGB stars of  $M \leq 3 - 4 M_{\odot}$  (hereafter Low Mass Stars, or LMS). In fact in LMS the maximum temperature at the bottom of TPs, though gradually increasing with the pulse number, barely reaches the above mentioned value. Despite the very low neutron exposure associated with its activation in LMS, the peak neutron density generated by the  $^{22}\text{Ne}$  source is rather high (up to  $n_n = 10^{10} \text{ cm}^{-3}$ ) and affects many branchings along the  $s$  path that are sensitive to the neutron density and/or to temperature (Käppeler et al. 1990; Arlandini et al. 1999). Notice that the final modifications on branching-dependent isotopes are important, since the  $s$ -processed and partially diluted matter is irradiated repeatedly and therefore keeps a partial memory of all the previous high-temperature phases.

In more massive AGB stars ( $5 < M/M_{\odot} < 8$ , hereafter Intermediate Mass Stars, or IMS),  $^{22}\text{Ne}$  burns efficiently through  $^{22}\text{Ne}(\alpha, n)^{25}\text{Mg}$  and  $^{22}\text{Ne}(\alpha, \gamma)^{26}\text{Mg}$  reactions, in roughly equal proportion, since the maximum bottom temperature in TPs is  $T \geq 3.5 \times 10^8$  K (Iben 1975; Truran & Iben 1977). As a consequence, a significant neutron exposure is made available. Simultaneous production of  $^{25}\text{Mg}$  and  $^{26}\text{Mg}$  occurs such that these isotopes are expected to be enhanced in the photospheres of AGB stars of intermediate mass. Moreover, the high peak neutron density ( $n_n > 10^{11} \text{ cm}^{-3}$ ) induces a considerable production of the few neutron-rich nuclei involved in those  $s$ -process branchings sensitive to the neutron density, such as  $^{86}\text{Kr}$ ,  $^{87}\text{Rb}$ , and  $^{96}\text{Zr}$ . Their abundance can be enhanced even more than for the  $s$ -only species. Moreover, IMS may suffer from the so-called hot bottom burning process (HBB) in the deep

convective envelope, which would decrease the photospheric  $^{12}\text{C}/^{13}\text{C}$  ratio and enhance the abundance of Li. It would also reduce the C/O ratio, thus preventing the star from becoming C-rich for most of its AGB phase (e.g., Lattanzio & Forestini 1999).

The observational evidence so far available points toward a relatively low peak neutron density in AGB stars ( $n_n < 10^8 \text{ cm}^{-3}$ ), as derived from the Sr/Rb abundance ratio and in a few cases from the Zr isotopic mix (Lambert et al. 1995). This can be interpreted as an indication that most intrinsic and extrinsic AGB stars are of rather low mass (Busso et al. 1988). The fact that AGB stars of intermediate mass are rather rare is then confirmed by the roughly solar isotopic ratio measured for Mg in MS and S giants (see e.g. Clegg, Lambert, & Bell 1979; Blanco, McCarthy, & Blanco 1980; McWilliam & Lambert 1988).

### 2.3. The Updated reference Models

Stellar models were computed using the FRANEC code (Straniero et al. 1997; G98) and spanned the metallicity range from solar down to 1/20 solar ( $1.5 M_\odot$ ) and from solar down to 1/3 solar ( $3 M_\odot$ ).

Our nucleosynthesis predictions, covering the metallicity interval from  $[\text{Fe}/\text{H}] = +0.3$  down to  $[\text{Fe}/\text{H}] = -3.6$ , were calculated as post-process runs, extrapolating the stellar parameters from the mentioned coarser grid of full evolutionary models. The differences in the physical structure of the He intershell are found to be small, even for models with large differences in the initial metallicities (see also Boothroyd & Sackmann 1988, 1999). The parameter most heavily affected by the metal content is the TDU, which is found to increase in efficiency for decreasing  $[\text{Fe}/\text{H}]$  values. For these reasons, the amount of dredge up at very low metallicities may be somewhat underestimated in our extrapolations, and TDU can occur also for masses lower than actually found. Mass loss was considered through the Reimers (1975) formula, varying its free parameter to obtain a wide range of parameterizations. The values considered in this paper are  $\eta = 0.3$  ( $1.5 M_\odot$ ),  $\eta = 1.5$  ( $3 M_\odot$ ). With the FRANEC code and its assumptions for convective mixing, TDU is found to cease when the residual envelope mass becomes smaller than about  $0.5 M_\odot$ , while thermal pulses are still going on. Given the uncertainties of the mixing procedure in stellar models, and of the mass loss rates, we cannot claim that this last finding is a common property of real AGB stars. However, on this point the different stellar codes tend to agree (see also Lattanzio & Karakas 2001). Should this correspond to a real physical property, then it would also imply that stars with too small envelope masses (hence also with too small *initial* masses) cannot undergo TDU, and cannot contribute to the chemical enrichment of the Galaxy (T99). The minimum initial mass at which TDU is found with the FRANEC code is  $1.5 M_\odot$  for a solar

composition, and decreases slightly for decreasing metallicity: however the uncertainty is high and the actual values should be tuned through comparisons with observations (see also § 3.2 and the discussion of Figure 7). Exceptional conditions have probably to be invoked to explain objects with unusual  $s$  enrichments, up to 1 order of magnitude higher than the maximum defined by common AGB stars: see e.g. the cases of F Sge (Gonzalez et al. 1997), the Sakurai’s object (Asplund et al. 1999) and in general the class of R CrB stars (Asplund et al. 2000). We also recall that in Paper I we analysed which would be the consequences of a prolonged interruption in the TDU process. We showed that, in this case, some MS or S stars without Tc might actually be intrinsic, Tc having decayed due to lack of refurbishing from the He intershell.

The first published models for  $^{13}\text{C}$  burning in AGB stars assumed that the neutrons were released from the reaction  $^{13}\text{C}(\alpha, n)^{16}\text{O}$  in convective conditions, after the  $^{13}\text{C}$  pocket was ingested by the next TP (Hollowell & Iben 1998; Käppeler et al. 1990). The resulting  $s$ -process nucleosynthesis was analysed to understand abundances in AGB stars of the Galactic disk (Paper I and Paper II). In such calculations, a repeated neutron exposure was achieved thanks to partial overlapping of material cycled through several TPs. Though more complex than in the simple original sketch by Ulrich (1973), the  $s$ -process mechanism could still be approximated by an exponential distribution of neutron exposures. We recall that the classical analysis of the *main* component represented by the solar-system  $s$ -process abundances in the atomic mass range  $A = 85 - 208$  (e.g., Käppeler, Beer & Wisshak 1989), assumed a distribution function of neutron exposures  $\rho(\tau) \sim \exp(-\tau/\tau_0)$ , where  $\tau$  is the time integrated neutron flux,  $\tau = \int n_n v_{th} dt$ ,  $v_{th}$  being the thermal velocity and  $n_n$  the neutron density (Seeger, Fowler, & Clayton 1965). The parameter  $\tau_0$  is called *mean* neutron exposure. According to Arlandini et al. (1999), the main component is best reproduced with  $\tau_0 = (0.296 \pm 0.003) (kT/30 \text{ keV})^{1/2}$ . As a matter of fact, previous AGB stellar models already showed that different  $s$ -element distributions were obtained by varying the amount of  $^{13}\text{C}$  in the pocket and/or the initial metallicity. In this respect, the observed spread of [hs/ls] values in Galactic disk MS and S stars was explained quantitatively by saying that they imply values of the *mean* neutron exposure  $\tau_0$  (expressed at 30 keV) in the range 0.2 – 0.4 mbarn $^{-1}$ . CH and Ba stars were found to extend the range of mean neutron exposures further, up to  $\tau_0 (30 \text{ keV}) \sim 0.8 - 1.0 \text{ mbarn}^{-1}$  (Paper II).

A reanalysis of AGB evolution was recently pursued by various authors (see e.g. Herwig et al. 1997; Herwig, Schönberner, & Blöcker 1998; Frost et al. 1998; Frost, Lattanzio & Wood 1998). We shall follow here the work by Straniero et al. (1997). They showed that all  $^{13}\text{C}$  nuclei present in the pocket are consumed locally in radiative conditions (over a time interval of a few  $10^4$  yr) when these layers are heated up to  $10^8$  K before the next convective instability sets in. The rate of the  $^{13}\text{C}(\alpha, n)^{16}\text{O}$  reaction (Denker et al. 1995) is rather uncertain at



the relevant temperatures ( $T \sim 0.9 \times 10^8$  K), but we expect complete exhaustion of  $^{13}\text{C}$  in the radiative interpulse phase for all reasonable values of the rate (Arlandini et al. 1999). In such conditions, the neutron fluxes are characterized by a rather low neutron density ( $n_n \leq 1 \times 10^7$  n/cm<sup>3</sup>), as a consequence of the relatively low temperature at which  $^{13}\text{C}$  burns. The effect of the recurrent convective instabilities is nevertheless of the highest importance, since they dilute the  $s$ -enriched material of the  $^{13}\text{C}$  pocket over the whole He intershell, allowing subsequent neutron-capture episodes to occur over a mixture containing fresh iron-seed nuclei and material already  $s$ -processed in the previous cycles. The ensuing chemical homogeneization of the He intershell also allows the neutron-rich nuclei to be mixed with the envelope by TDU.

The fact that  $^{13}\text{C}$  burns radiatively in the interpulse period makes the  $s$  process more complex than previously assumed. Further complications are due to the fact that the mass involved in each thermal pulse decreases with time, as the core mass increases, while the overlapping factor  $r$  between adjacent pulses decreases with pulse number. The ensuing neutron exposure is much closer to a superposition of few single irradiations than to an exponential distribution of neutron exposures (see G98 for further details).

For the sake of our comparisons with observed stars, we adopt a wide range of  $^{13}\text{C}$  abundances in the pocket. We include the case indicated as standard (ST) by G98, corresponding to  $4 \times 10^{-6} M_\odot$  of  $^{13}\text{C}$ , and values scaled upward (by a factor 2) and downward (by factors 1.5, 3, 6, 12 and 24) with respect to that choice. The ST case was so named because this amount of  $^{13}\text{C}$  for AGB stars in the mass range  $1.5 - 3 M_\odot$  at  $[\text{Fe}/\text{H}] = -0.3$  appears to explain the main (solar) component of the  $s$  process (Arlandini et al. 1999). Notice that the same result can be obtained by varying simultaneously the metallicity and the amount of  $^{13}\text{C}$  in the pocket provided the ratio  $^{13}\text{C}/\text{Fe}$  remains constant; this ratio essentially fixes the number of neutrons available per heavy seed. It is, however, clear that both the particular  $s$ -element distribution achieved in the Sun and the spread of  $s$ -process abundances observed in chemically unevolved stars at each metallicity (i.e. stars that have maintained their initial composition) should be considered as the result of a complex chemical evolution of the Galaxy, through the astration mechanism over various generations of AGB stars of different masses, metallicities, and  $s$ -process efficiencies.

## 2.4. Metallicity effects in the models

For each choice of the  $^{13}\text{C}$  pocket and stellar mass, the  $s$ -process efficiency in the He intershell varies according to the initial metallicity. Figures 1 and 2 show the overproduction factors of stable elements from Cu to Bi in the material cumulatively mixed from the He

intershell to the envelope. The results refer to the ST choice for the  $^{13}\text{C}$  pocket for AGB models of  $1.5 M_{\odot}$ , metallicity varying from  $[\text{Fe}/\text{H}] = +0.3$  down to  $[\text{Fe}/\text{H}] = -0.6$  (Figure 1) and from  $[\text{Fe}/\text{H}] = -1$  down to  $[\text{Fe}/\text{H}] = -3$  (Figure 2). In these figures, the elements represented by bold symbols owe more than 50% of their solar abundance to the  $s$  process, according to the analysis by Arlandini et al. (1999). The remaining elements are indicated as crosses. The elements used here to build the ‘hs’ and ‘ls’ integrated abundances are indicated explicitly in the third panel of Figure 1. In the  $s$ -processed material mixed with the envelope, the unstable nuclei with half-life longer than an interpulse period (typically between  $10^4$  and  $10^5$  yr in LMS) but shorter than  $10^9$  yr, have been allowed to decay, as expected for extrinsic AGB stars. For comparison, the abundances before such decays are shown as open symbols (squares for the mainly- $s$  elements). The isotopes involved are the pairs  $^{93}\text{Zr} - ^{93}\text{Nb}$ ,  $^{99}\text{Tc} - ^{99}\text{Ru}$ ,  $^{107}\text{Pd} - ^{107}\text{Ag}$ ,  $^{135}\text{Cs} - ^{135}\text{Ba}$ ,  $^{205}\text{Pb} - ^{205}\text{Tl}$ . It is clear from the figures that the element distribution is strongly dependent on the initial composition. They show how the light  $s$  elements belonging to the Zr-peak are preferentially produced at nearly solar metallicities. At lower metallicities, like those of the old Galactic disk (e.g.  $-0.8 \leq [\text{Fe}/\text{H}] \leq -0.6$ ), the Ba-peak elements become dominant. This is so because the neutron exposure increases with decreasing iron seed abundances. For the most metal-poor stars (Figure 2) the flow along the  $s$ -process path accumulates on  $^{208}\text{Pb}$ , the doubly-magic nucleus at the termination point of the  $s$ -path, and partly on  $^{209}\text{Bi}$ . Similar trends are observed for the other choices of  $^{13}\text{C}$  in the pocket.

It is from the averaging of very different contributions, like those illustrated in Figures 1 and 2, that Galactic chemical evolution generates the heavy  $s$ -elements in the solar system (T99). The trends of these figures show that a progressively increased production of Pb is to be expected at the surface of AGB stars with decreasing  $[\text{Fe}/\text{H}]$ , at the expense of both the Zr-peak (ls) and the Ba-peak (hs) elements. Therefore, for halo stars, all criteria based solely on these last two parameters lose their meaning. AGB stars of low metallicity are the major producers of Galactic Pb (G98; Travaglio et al. 2001), and represent the astrophysical site of the so-called *strong* component advanced by the classical analysis (Clayton & Rassbach 1967).

## 2.5. Surface abundances and their dependence on metallicity

Using the AGB models with mass loss prescriptions described above, we computed the envelope compositions for each stellar mass and metallicity after each TDU episode, from the first occurrence of mixing with the envelope (after a limited number of TPs, see Straniero et al. 1997) to the end of the AGB phase. This allows us to build a large data bank of

model abundance distributions, evolving pulse after pulse, characterized by three different parameters (initial mass of the parent star, abundance of  $^{13}\text{C}$  in the pocket, metallicity).

In Figures 3 (a, b, c) and 4 (a, b, c), we show predicted values of  $[\text{hs}/\text{ls}]$ ,  $[\text{ls}/\text{Fe}]$ , and  $[\text{hs}/\text{Fe}]$  in the photosphere at the last TDU episode for the 1.5 and 3  $M_{\odot}$  stellar models. The non-linear trends displayed by the plots reveal the complex dependence on metallicity of the integrated abundances ‘ls’ and ‘hs’. This is due to the neutron exposure, which increases with decreasing abundance of the iron seed nuclei. To illustrate this, let us follow the ST case. Starting at metallicities higher than solar and moving toward lower  $[\text{Fe}/\text{H}]$  values, a minimum with  $[\text{hs}/\text{ls}] = -0.54$  is first reached at  $[\text{Fe}/\text{H}] = 0.2$  (the Zr-peak elements are more abundantly produced for moderate exposures, hence for relatively high metallicities). Then a maximum with  $[\text{hs}/\text{ls}] = 1.2$  follows at  $[\text{Fe}/\text{H}] = -1$ . Finally, for even lower metallicities, the *s*-process flow extends beyond the Zr-peak and Ba-peak nuclei to cause an accumulation at  $^{208}\text{Pb}$ , and  $[\text{hs}/\text{ls}]$  declines again. Reducing the amount of  $^{13}\text{C}$  burnt has the effect of displacing the maximum and the minimum of the curve toward lower metallicities. Note that the maxima reach values in  $[\text{hs}/\text{ls}]$  up to 1.2, consistently higher than in all previous expectations. The minima reach down to  $-0.7$ , at a  $[\text{Fe}/\text{H}]$  value depending on the  $^{13}\text{C}$  choice.

At extremely low  $[\text{Fe}/\text{H}]$  values, the scarcity of Fe nuclei becomes important. Here their role as seeds for the *s*-process is replaced partly by lighter (intermediate atomic mass) nuclei, whose abundances remain high due both to the known enhancement of  $\alpha$ -rich elements in halo stars and to the fact that they are synthesised from primary  $^{12}\text{C}$  generated in the He intershell and mixed with the envelope by TDU. When this  $^{12}\text{C}$  is transformed into  $^{14}\text{N}$  by the H-burning shell, it provides more fuel for the chain  $^{14}\text{N}(\alpha, \gamma)^{18}\text{F}(\beta^+ \nu)^{18}\text{O}(\alpha, \gamma)^{22}\text{Ne}$  early in the TP. The nuclei that are progeny of  $^{22}\text{Ne}$ , usually considered merely as neutron filters (or ‘poisons’) at higher metallicities, now assume a more complex role. Neutron captures on them generate a small leakage that crosses the iron peak, thus allowing the *s* processing on heavy isotopes to continue.

Due to the above phenomena, the *s* nuclei cannot be considered as being simply of ‘secondary’ nature. It is true that they require previously built seeds to be formed, but at moderately low metallicities their secondary behavior is masked by the increase in the neutron exposure, on which the resulting *s*-process abundances strongly depend (Clayton 1988). At very low  $[\text{Fe}/\text{H}]$  values part of the seeds feeding them are primary, so that they achieve a trend that only slightly decreases for decreasing  $[\text{Fe}/\text{H}]$ .

## 2.6. Sensitivity of the results to model parameters of $^{13}\text{C}$ burning

Neutrons released by the  $^{13}\text{C}$  neutron source are captured locally in the  $^{13}\text{C}$  pocket. Only after their ingestion in the next TP are the  $s$  enriched layers of the  $^{13}\text{C}$  pocket mixed together and spread over the (now convective) He intershell. To better understand how this complex mechanism occurs, and to study its sensitivity to input parameters, we consider in some detail the behavior of  $s$ -processing in the various layers of the  $^{13}\text{C}$  pocket together with the effects of mixing and dilution operated by TPs. For any  $^{13}\text{C}$  neutron burst, the starting composition of Fe seeds and heavy elements in the pocket is not the initial one, but rather the composition left behind by the operation of previous TPs (see Figure 5), already highly enriched in heavy elements.

This is illustrated schematically in Table 1, where the evolution of three representative isotopes of the Zr, Ba, and Pb peaks are followed for the model of an AGB star of  $1.5 M_{\odot}$  and solar metallicity, adopting the ST choice for the  $^{13}\text{C}$  pocket. The relevant zones of the stellar structure are shown in Figure 5. For illustration let us consider the layers in the pocket of initial abundance  $X(^{13}\text{C}) = 0.003$  and  $0.004$ . Column 1 gives the TP number (with TDU) that precedes the corresponding  $^{13}\text{C}$ -formation episode, column (2) indicates the zone to which the abundances refer: layer 1 and layer 2, as indicated in the figure, then the average in the  $^{13}\text{C}$  pocket at the end of the interpulse phase (zone 3 in the figure), and finally the average at the end of the next TP (labeled as ‘4’ in the figure). The composition of this last region includes the effects of dilution over the extension of the convective He intershell, with material from upper layers containing ashes of H-shell burning, and material from lower layers already  $s$ -processed in the previous TP cycles. During each TP one has to take into account also the small neutron burst by the  $^{22}\text{Ne}$  source, but this affects only marginally the production of  $^{94}\text{Zr}$ ,  $^{138}\text{Ba}$ , and  $^{208}\text{Pb}$ . Column 3 gives the mass (in solar units) affected by the next convective TP, column (4) gives the neutron exposure  $\delta(\tau)$  (in  $\text{mbarn}^{-1}$ ), where  $\delta(\tau) = \int n_n v_{th} dt$  is integrated over the interpulse period. Typical thermal conditions during  $^{13}\text{C}$  consumption correspond to  $kT = 8$  keV. Column (5), (6), and (7) give the production factors of  $^{94}\text{Zr}$ ,  $^{138}\text{Ba}$ ,  $^{208}\text{Pb}$  relative to solar (Anders & Grevesse 1989). Although the three selected isotopes are not of purely- $s$  origin, they owe most of their production to the  $s$ -process. Following their synthesis as a function of pulse number in the two selected zones, we note how in the first cycle a small difference in  $\delta(\tau)$  in the two regions gives rise to a huge difference in their production factors. This lets the highly non-linear trend of the  $s$ -process efficiency to show up. However, the ratio of the production factors between the two zones is progressively smoothed in the subsequent TPs. For  $^{94}\text{Zr}/^{94}\text{Zr}_{\odot}$  it goes from 0.21 in the first  $^{13}\text{C}$ -burning episode to 0.66 in the 5<sup>th</sup> and to 0.73 in the 20<sup>th</sup>. For  $^{138}\text{Ba}/^{138}\text{Ba}_{\odot}$  the range is from 0.47 to 0.55 and to 0.64, respectively. (See G98 for a discussion of asymptotic conditions reached in advanced TPs). Concerning  $^{208}\text{Pb}$ , the production of this isotope at

the termination of the  $s$ -process path grows with pulse number more slowly than the nuclei at the other two  $s$ -process peaks.

The neutron exposures listed in column (4) show a slight decline with increasing pulse number in both selected layers. This smoothing effect is due to the repeated averaging of the  $s$ -process products operated by the TPs, which dilute the  $s$ -enriched layers in the way described above, over a stellar zone that contains about twenty times more mass than the one where neutrons are produced. Due to these extreme and repeated dilutions, even large variations in local details of the pocket have only small effects on the final distribution of the  $s$  elements, as our calculations demonstrate. In fact, we repeated the whole series of nucleosynthesis computations for different metallicities just assuming, for each choice of the total  $^{13}\text{C}$  concentration, the simplest possible profile, i.e. a constant abundance throughout the pocket. In this exercise a mass fraction  $X_{13} = 0.004$  represents the "smoothed" ST case. The resulting  $[\text{hs}/\text{ls}]$  trend versus metallicity is shown in Figure 6. When comparing it with the previous behavior (Figure 3a), it immediately appears that the two sets of results are almost indistinguishable. This gives us confidence in the results, even in the absence of a self-consistent model for the formation of the  $^{13}\text{C}$  pocket.

### 3. Observations of $s$ -process Enrichment in Disk and Halo Stars

#### 3.1. Unevolved Stars

In our comparisons with compositions of  $s$  enriched stars, we involve both intrinsic and extrinsic AGBs. Use of indices such as  $[\text{ls}/\text{Fe}]$ ,  $[\text{hs}/\text{Fe}]$ , and  $[\text{hs}/\text{ls}]$  calls for an assumption about the initial values of them. It is common to assume that the star, while on the main sequence, had  $[\text{ls}/\text{Fe}] = [\text{hs}/\text{Fe}] = [\text{hs}/\text{ls}] = 0$ . These initial conditions are also adopted in the theoretical calculations. Given the increasing quality of the observational data and the sophistication of the models it is worthwhile to review the evidence on heavy element abundances in disk and halo stars.

Intrinsic, that is single AGB and post-AGB stars, build up their  $s$  enrichments as they experience successive TDUs. One predicts the enrichment and  $[\text{hs}/\text{ls}]$  to evolve as the AGB evolves. This evolution should be observable through abundance analyses of a large sample of intrinsic stars. Extrinsic stars gain their  $s$  enrichments by mass transfer from an AGB companion. Then, the measured  $[s/\text{Fe}]$  refers to the average  $s$ -processed material of the AGB star after dilution by mixing with the envelope of the presumed unevolved companion that is now the extrinsic,  $s$ -enriched star. If, as is often the case, considerable  $s$ -processed material is transferred, the initial composition of the star is effectively irrelevant and the

observed [hs/ls] is the one of the material transferred to the secondary component. Again, predictions for [s/Fe] and [hs/ls] are testable using compositions of extrinsic stars.

Enrichments are quoted relative to the solar composition scaled to the metallicity of the star. Hence [ls/Fe] denotes the enrichment provided that [ls/Fe] = 0 for an unevolved star of that metallicity [Fe/H]. This certainly appears to be the case for stars with [Fe/H]  $\geq$  -1, but more metal-poor stars present an interesting issue, especially those with [Fe/H]  $\leq$  -2.5.

Edvardsson et al. (1993) showed that in their sample of disk stars ([Fe/H] > -0.8), relative abundances ([s/Fe]) were solar to within about 0.1 dex. Studies of more metal-poor stars were reported by Zhao & Magain (1991) for Y and Zr, and Gratton & Sneden (1994) for a sample of ls and hs elements. In the range [Fe/H] of -1 to -2, there do appear to be slight departures from [s/Fe] = 0. Gratton & Sneden report mean values from a combination of their data with that of Zhao & Magain’s measurements:  $\langle [s/Fe] \rangle = +0.07$  (Sr),  $-0.17$  (Y),  $+0.20$  (Zr) for the light-*s* elements, with uncertainties ( $\sigma$ ) of individual values of about 0.1 dex. For heavy-*s*, Gratton & Sneden from their own results give  $\langle [s/Fe] \rangle = -0.08$  (Ba),  $-0.11$  (La),  $+0.04$  (Nd),  $+0.14$  (Sm), also with an uncertainty of about 0.1 dex. Standard errors of these means are about 0.04 dex. These uncertainties are so much smaller than those associated with the measurement of abundances in intrinsic and extrinsic *s*-enriched stars that we ignore the small corrections that might be applied to the measured [s/Fe] to account for departures from [s/Fe] = 0 in the star’s original material. One exception to this is made when attempting to reproduce the detailed distribution of abundances, including several elements, as in the three cases discussed in § 4.

Metal-poor stars with [Fe/H] < -2.5 show an extraordinary range in heavy element abundances (McWilliam et al. 1995, 1996; Ryan, Norris, & Beers 1996; McWilliam 1997, 1998). At a given [Fe/H], ratios such as [Sr/Fe] and [Ba/Fe] range over 2 dex or more, from almost -2 to +1. McWilliam (1998) showed that [Ba/Eu] has essentially a unique value despite the enormous range in their abundances (relative to Fe) with that value being the solar *r*-process value. Most of the stars have a solar *r*-process mix of heavy elements, a mix inherited from their natal clouds that were contaminated by ejecta from perhaps one or two Type II SNe. In light of the large range in the heavy element to iron abundances, a signature of severe *s*-processing may not always be evident; for example, addition of substantial amounts of *s*-processed material to a star having an initial [Ba/Fe]  $\sim$  -2 could still leave the star with a [Ba/Fe] less than the maximum shown by unevolved stars. With certain assumptions (i.e., Eu is purely a *r*-process product and the *r*-process nuclides are present in solar proportions), it is possible to attempt a resolution of the elemental abundances into *s*- and *r*-process contributions (Burriss et al. 2000). These attempts may however be hampered by the recognized bimodal distribution of *r*-elements, the lighter species (with atomic mass

weight below 130-140) being produced by a different and rarer subclass of Type II supernovae than the heavier nuclei (Wasserburg & Qian 2000). In this paper, we restrict discussion to stars with a [Ba/Fe] well outside the range spanned by the majority of the very metal-poor stars. We further eliminate stars for which severe enrichment by the  $r$ -process is the more plausible explanation. A few stars do appear to be highly enriched in  $s$ -process products. These are either stars on the main sequence or low luminosity red giants, i.e. they are either binary (e.g., metal-deficient Ba stars) or were born out of gas enriched with ejecta from AGB stars. In the latter case, the meaning of ‘extrinsic’ must be extended and should not be assumed as always synonymous with mass transfer binary. The only possibility that such stars are intrinsically  $s$ -enriched is that a neutron source is tapped prior to the AGB phase. The He-core flash is a conceivable suspect, but models have not so far confirmed this idea. The enormous range in [s/Fe] at a given [Fe/H] is a complicating factor in the identification and interpretation of  $s$ -enriched stars, whether intrinsic or extrinsic.

### 3.2. $s$ -Enriched Stars of the Galactic Disk and Halo

Galactic-disk  $s$ -enriched stars, here [Fe/H]  $> -1$ , were considered in Paper II. They include the intrinsic MS and S stars with technetium, and the cool carbon stars. Extrinsic stars include MS/S stars with no Tc, the Ba II giants, and the CH subgiants. Here, we collate the observational results of the highest quality. With two exceptions, we limit discussion to analyses based on spectra recorded on Reticons or CCDs. The two exceptions are Smith’s (1984) survey, and the use of Tech’s (1971) results for  $\zeta$  Cap by Smith & Lambert (1984). Among the now excluded stars are the cool carbon stars for which heavy element abundances are uncertain owing to severe molecular line blanketing. For halo stars, here [Fe/H]  $< -1$ , we gather results from the literature. The observed values for the parameters [ls/Fe], [hs/Fe], [hs/ls] are listed in Table 2, together with references to the original observations. This table forms the set of observational constraints to theoretical predictions, extending over the whole metallicity range in the Galaxy. We have attempted to separate the stars into the categories extrinsic and intrinsic.

Brief remarks on the stars in Table 2 follow: the sample is certainly not complete, but we hope it is at least as homogeneous as possible, and takes into account the most representative  $s$ -enhanced sources in the Galaxy. In our comments below we begin with several classes of what are considered to be intrinsic stars:

**MS/S stars with Tc, Table 2a.** For a sample of intrinsic stars of disk metallicity, we select the MS and S stars that exhibit Tc lines in their spectra. Presence of Tc implies that these stars are experiencing TDUs, i.e., are intrinsically  $s$  enriched. Smith & Lambert

(1985, 1986, hereafter SL85 and SL86) and SL90 analysed 11 MS/S stars and a sample of normal M stars differentially with respect to the late-K giant  $\alpha$  Tau. The result that the normal M stars gave the indices [ls/Fe], [hs/Fe], and [hs/ls] very close to zero in the mean, with a small scatter, implies that the abundance obtained for the MS/S stars are reliable. In the stars from SL90, only Nd was measured among the ‘hs’ elements, and its abundance is reported in Table 2a. In the other stars from SL85, SL86, Ba and Nd were used to define the ‘hs’ parameter and we follow this choice.

**SC Stars, Table 2a.** Abia & Wallerstein (1998) analysed seven SC stars and four S stars. Their abundances of the heavy elements are consistent from one star to the next, but are somewhat unusual compared to other intrinsic and extrinsic stars. For [ls/Fe] and [hs/Fe] we find, using Y and Zr, and La and Nd (where measured) means from six stars of +1.1 and +1.2 for an average [Fe/H] of 0.1 dex. More typical values in S giants are around 0.6 dex for these quantities. The differences for SC stars might in principle be due to a more advanced evolutionary stage, in which the C enrichment has (almost) reached the condition C/O = 1. As expected, the mean [hs/ls] index is less affected and the average value of 0.0 is more consistent with that from other AGB stars. We must however mention that the spectra of these SC/S stars are very complex, and rich in CN lines in the red regions analysed by Abia & Wallerstein. The difficulty of identifying and measuring weak atomic lines on these spectra of intermediate resolution is another possible explanation for the apparently anomalous composition deduced. As an illustration of the impact of line blending, we note that few Fe I lines were measured: the sample ran from one line in BH Cru and GP Ori to a maximum of 11 for CY Cyg. Very few of the Fe lines were weak. Our conjecture is that the Fe abundances might have been overestimated, which would account for the fact that 5 of the stars had [Fe/H]  $\geq$  0.2. The fact that reference stars - the M2.5II-III standard  $\beta$  Peg and the K5III star  $\theta$  UMi - gave credible results provides partial confirmation of the analytical techniques, but the spectra of these stars are not severely impacted by molecular line blanketing. A recent analysis of C(N) stars by Abia et al. (2001) further discusses the uncertainties in measuring C-rich spectra and partially reconsiders the SC data, suggesting the possibility of unidentified blends affecting the quantitative results. Due to this, we give lower weight to the results for these SC/S stars and represent them collectively, through their mean abundances (see Table 2a and Figures 7, 8, and 9).

**Post-AGB C-rich Stars, Table 2a.** The label ‘post-AGB’ is applied to a variety of luminous warm stars. Here, we pick out those that are rich in carbon with most identified from IRAS surveys as showing a 21 $\mu$ m broad emission feature. Six stars were analysed by Van Winckel & Reyniers (2000), two by Reddy, Bakker, & Hrivnak (1999), and one by Začs, Klochkova, & Panchuk (1995). These span the metallicity range [Fe/H] =  $-0.3$  to  $-1.0$  and, hence, are not Galactic halo stars by our simple classification. All are assumed



to be intrinsic stars on account of their C and *s*-enrichment, attributed to TDUs when on the AGB. Assuming that departure from the AGB driven by envelope reduction through a stellar wind occurred after the envelope has attained its asymptotic mix of *s* elements (i.e., [hs/ls] is then a constant independent of the number of TDUs, but [*s*/Fe] continues to increase), the *s*-process enrichment traces the terminal ratio [hs/ls] as a function of [Fe/H], and, perhaps, also the number of TDUs as a function of [Fe/H] before the star leaves the AGB. We comment further on these relations later.

**Intrinsic metal-poor carbon stars, Table 2b.** A series of analyses on such stars have been reported by Kipper and colleagues. Kipper et al. (1996) discuss five stars with [Fe/H] between  $-0.7$  and  $-1.15$ . Kipper & Jørgensen (1994) analysed a much more metal-poor star ([Fe/H] =  $-2.5$ ). Two earlier analyses (Kipper & Kipper 1990; Kipper 1992), not included in our Tables because they were based on photographic spectra, were also of very metal-poor stars, [Fe/H] =  $-2.8$  for HD 13826 (V Ari), and  $-2.9$  for HD 112869 (TT CVn). Interpretation of these results must bear in mind that molecular line blanketing in the spectra of these cool giants is severe and, even in the case of the most metal-poor stars, limits the accuracy of the elemental abundances: ‘metal abundances have quite large errors amounting to 0.5 dex due to extremely heavy blending of most metal lines by molecular lines’ (Kipper & Jørgensen 1994) but ‘in some cases’ (say Fe) may be 0.2 dex. The nature of blending-based errors is such that they cannot always be expected to be reduced in forming ratios such as [hs/ls]. As in the case of SC stars, we assign therefore lower weight to such results. The status of these stars is a little uncertain. Despite their temperatures, somewhat in excess of those for typical AGB stars, ‘Possibly all cool halo carbon stars may have formed as intrinsic carbon stars’ (Kipper et al. 1996). We therefore suppose them to be intrinsic, though this assumption should be better checked in the future. Being old objects, they should be of rather low mass, but TDU becomes more efficient for low metallicities, so that the C-star phenomenon might extend to lower masses for halo stars. Indeed it is known that the number ratio between C stars and M giants increases at low metallicity. They are rich in  $^{13}\text{C}$ , like the rather common CJ stars: this can however be understood at low mass through the operation of Cool Bottom Processes (CBP: see Wasserburg, Boothroyd, & Sackmann 1995). Notice that, according to Kipper et al., the stars in Table 2b have to be considered as belonging to the halo, even if their metallicity does not always obey the rule  $[\text{Fe}/\text{H}] \leq -1$ . As the highest metallicities of the Galactic halo and the lowest of the Galactic disk partially overlap, this rough discrimination is in this case insufficient. The same comment apply to HD 209621 (see later Table 2d).

**Extrinsic stars in the Galactic disk, Table 2c.** We include here MS and S stars without Tc in their spectra, which are supposed to be evolved versions of barium stars. Indeed, abundance analyses by SL85, SL86, SL90. show that they have *s*-enrichments like

those of Ba II K-type giants. The same rules discussed for MS/S stars with Tc on the selection of ls and hs abundances apply here. We also consider the CH subgiants analysed by Smith et al. (1993), and Ba II giants from several sources (Smith 1984; Smith & Lambert 1984; Tomkin & Lambert 1983, 1986; Kovács 1985; Smith & Suntzeff 1987). For CH subgiants, we include Ba and Nd in the ‘hs’ index, as done by Smith, Coleman, & Lambert (1993). Due to our already mentioned choices on the type of observations to include, we omit extrinsic stars from Luck & Bond (1984, 1985, 1991a,b), because abundances were derived from photographic spectra. As shown elsewhere (see e.g. Busso & Gallino 1997), those abundances can be in general well explained by AGB models; they however give constraints qualitatively similar to those already provided by our more homogeneous set of data. In the class of extrinsic Galactic disk stars we may include also the K giant BD +75°348 (Začs, Schmidt, & Schuster 2000), which has  $[\text{Fe}/\text{H}] = -0.8$  and *s* enrichment similar to those of an extreme Ba II star. One supposes it is a spectroscopic binary but radial velocity measurements are presently lacking.

#### **Extrinsic Galactic halo AGB stars, Table 2d**

In the group of Galactic halo extrinsic stars we include the objects described below.

**CH giant stars.** A sample of these stars, the metal-poor or halo counterpart of the classical Ba II giants, were analysed by Vanture (1992). Abundances of heavy elements were reported for seven stars with  $[\text{Fe}/\text{H}]$  from  $-0.9$  to  $-1.7$ . A revision for HD 187861 was also suggested by Vanture (2000, private communication). Their status as ‘extrinsic’ is confirmed by their designation as spectroscopic binaries (McClure 1983, 1984). Owing to the larger uncertainty in abundance determinations in these stars (in particular HD 209621 and HD 221959), we assign lower weight to these results.

**Yellow symbiotic stars.** Three such stars have been analysed recently: AG Dra (Smith et al. 1996), BD  $-21^{\circ}3873$  (Smith et al. 1997), and He2–467 (Pereira, Smith, & Cunha 1998). ‘Yellow’ denotes that the giant has a spectral type of G-K and, hence, its spectrum is not cluttered with the TiO lines found in redder symbiotic stars. It is fair to presume that the giant has accreted material from its companion, which is now a white dwarf but earlier was a mass-losing AGB star.

**HD 196944.** Začs, Nissen, & Schuster (1998), who analysed this star, considered it ‘unlikely’ that it is a post-AGB star and place it as a peculiar AGB star or a CH star (i.e., extrinsic).

**LP 625-44, LP 706-7, and CS 22898-027.** The first is a C-rich star with  $[\text{Fe}/\text{H}] = -2.7$ , analysed by Norris et al. (1997) and Aoki et al. (2000). With  $[\text{Ba}/\text{Fe}] = +2.7$ , it is about 2 dex more Ba-rich than the most Ba-rich ‘normal’ metal-poor stars (McWilliam et

al. 1995), and the ratio  $[\text{Ba}/\text{Eu}] = 0.8$  implies  $s$ -process enrichment rather than  $r$ -process contamination (for which  $[\text{Ba}/\text{Eu}] = -0.8$  in the solar case, which seems to be representative of the heaviest elements in metal-poor  $r$ -process-dominated stars). Aoki et al. consider, partly on the grounds of radial velocity variations, the star to be the ‘result of mass transfer in a binary system from a previous AGB companion’ (i.e., LP 625-44 is an extrinsic star.). Abundances are taken from Aoki et al. It is clear that abundances from Ba to Pb follow the pattern expected of  $s$ -processing in a metal-poor AGB star of low mass. The low abundance of Europium, a traditional tracer of the  $r$ -process, is well fit by the predictions of the marginal  $s$ -process contribution, which amounts to only 5% of solar Eu. The C-rich star LP 706-7 (Norris et al. 1997) with  $[\text{Ba}/\text{Fe}] = 2.0$  is similar to LP 625-44, but slightly less evolved. It might be considered extrinsic, but proof in the form of radial velocity variations is presently lacking. CS 22898-027 (McWilliam et al. 1995; McWilliam 1998) is similarly C-rich and  $s$ -process enriched.

In contrast to this trio, there are stars, even C-rich stars, whose pattern of heavy element overabundances is that of the  $r$ -process. The best known examples are CS 22892-052 (Snedden et al. 1996), HD 115444 (Westin et al. 2000), and CS 31082-001 (Cayrel et al. 2001; Hill et al. 2001), but other similar objects exist (see e.g. Hill et al. 2000; Barbuy et al. 1997). Relative abundances of the heavy elements Ba to Pb match well the solar  $r$ -process abundances; the low  $[\text{Ba}/\text{Eu}]$  ratio is that expected of a solar-like  $r$ -process. Any possible  $s$ -process contribution to the abundances is swamped by the dominant  $r$ -process contribution. It should be noted that in very metal-poor stars, while the relative abundances of heavy elements are remarkably similar to those in the solar  $r$ -process, the ratio of the heavy- $r$  to light- $r$  elements is variable from star to star (Qian, Vogel, & Wasserburg 1998; Burris et al. 2000, Qian & Wasserburg 2001). As mentioned, this has been interpreted in the framework of a bimodal  $r$ -process, coming from supernovae of different frequency (Wasserburg & Qian 2000, Sneden et al. 2000).

A pair of stars showing evidence of carbon (and nitrogen) enrichment with heavy element abundances intermediate between pure solar  $r$ -process and an  $s$ -process was analysed by Hill et al. (2000). That the ratio  $[\text{Ba}/\text{Eu}] \simeq 0.0$  is intermediate between that of the  $r$ -process dominated CS 22892-052 ( $\simeq -0.8$ ) and that of the  $s$ -process dominated LP 624-44 ( $\simeq +0.8$ ) implies the atmospheres of the pair are a blend of  $r$ - and  $s$ -processed material. Unfortunately, the mentioned fact that there is not a unique set of  $r$ -process abundances for light and heavy elements bedevils attempts to resolve the abundances of Hill et al.’s stars into their  $r$ - and  $s$ -process components. In particular, the star-to-star variation in the ratio of the light  $r$ - to heavy  $r$ -elements necessarily compromises the extracted ratio of the light  $s$  to heavy  $s$  elements. Until the star-to-star variation is better understood, selection of  $s$ -process enriched very metal-poor stars is limited to those stars where the  $s$ -process is obviously dominant.

Although the present sample is extremely small, there is a tantalising hint that the  $r$ -process enriched stars like CS 22895-052 are giants, and the  $s$ -process enriched stars like LP 625-44 are dwarfs or subgiants.

**N-rich subdwarfs: HD 25329 and HD 74000.** The rare class of N-rich subdwarfs was discovered by Bessell & Norris (1982). Beveridge & Sneden (1994) analysed two of these stars. For HD 25329, they determined the abundances of 9 heavy elements but for HD 74000 just 3 heavy elements were measured. These stars have metallicities of  $-1.8$  and  $-2.1$ , respectively. An  $s$ -process enrichment is indicated for HD 25329; too few elemental abundances were given for HD 74000 to make a similar assertion. The heavy elements, as well as the N, Na, and Al enrichments were attributed to synthesis in an AGB star but lacking direct evidence for a companion, the possibility of contamination of the natal clouds was left open.

### 3.3. Observation and Theory

Estimates of  $[\text{ls}/\text{Fe}]$ ,  $[\text{hs}/\text{Fe}]$ , and  $[\text{hs}/\text{ls}]$  were made for the stars in the previous section. Our estimates may differ from published values because we elect to consider a different mix of elements. The differences are slight and the overall conclusions drawn from the assembled data are unaffected by whether the original or our choices of heavy elements are adopted. We adopt in general the published estimates of  $[\text{Fe}/\text{H}]$ : exceptions are MS/S giants, where we make use of the more reliable  $[\text{M}/\text{H}]$  values, ‘M’ indicating an average from Ti to Fe. Using this average changes only slightly the values of  $[\text{ls}/\text{Fe}]$  and  $[\text{hs}/\text{Fe}]$ . Here, we compare the  $s$ -process indices against theoretical predictions.

Run of  $[\text{hs}/\text{ls}]$  versus  $[\text{Fe}/\text{H}]$  is shown in Figure 7, where filled and unfilled symbols refer to intrinsic and extrinsic stars, respectively. The two N-rich subdwarfs are shown by asterisks. Theoretical predictions for ST/1.5 (bold line) provide an approximate average fit to the data. For a comparison, two more lines, representing the envelope of our maximal and minimal predictions for  $[\text{hs}/\text{ls}]$  (as deduced from Figure 3a) are shown as dashed and dotted lines, respectively. This makes clear that most observed data are explained, within the errors, by model curves. The most remarkable outliers in Figure 7 are four C-rich objects with  $[\text{Fe}/\text{H}] \leq -2$  (one probably intrinsic, three probably extrinsic). They are CS 22898-027, LP 625-44, and LP 706-7 and HD 187216. The first has been already commented upon: absence of Y and Zr makes its data rather uncertain in our picture. The last was recognized as a puzzle difficult to accommodate in any explanation based on LMS evolution/nucleosynthesis already by Kipper & Jørgensen (1994), but has a complex spectrum and larger-than-average error bars should be attributed to its abundances. LP 625–44 was recently analysed by Ryan et

al. (2001), who found the distribution of *s*-elements from Ba to Pb in remarkable agreement with nucleosynthesis predictions from very low mass stars ( $M \leq 1.3 M_{\odot}$ ). The same may hold for LP 706–9, but spectra of higher resolution are needed. A very low initial mass, in connection with possible large inhomogeneities in the parent ISM at low metallicities, might be invoked for explaining the whole set of abundances in these extreme halo C-rich objects. We have problems in the fits also with IRAS 22272+5435, a post-AGB supergiant from Začs, Klochkova, & Panchuk (1995). However, this star has a large uncertainty in its metal abundances (e.g., Fe is deficient, the other elements of the Fe group are overabundant, the *s*-element abundances have uncertainties up to 0.5 dex) so that we must attribute a lower weight to it.

Conversion of a normal star to an extrinsic star by mass transfer from an AGB companion is not expected to change the [hs/ls] index. This expectation assumes that there is no differentiation/fractionation during the transfer of mass. Certainly, if dust and gas in the stellar wind are transferred and accreted differently, one might expect a difference owing to the selective condensation of elements into and onto grains. A cautious interpretation of Figure 7 is that intrinsic and extrinsic stars follow similar trends of [hs/ls] versus [Fe/H]. There is a suspicion voiced first by Reddy et al. (1999) and Van Winckel & Reyniers (2000) that the intrinsic post-AGB C-rich stars have a lower [hs/ls] than the Ba II stars and the CH giants. The two N-rich subdwarfs stand apart from the remainder of the sample, and are also distinguished by quite mild *s* enrichments, explained only by models with the lowest  $^{13}\text{C}$  concentration in the pocket. In what follows, we consider them separately from the majority of the sample.

Indices [ls/Fe] and [hs/Fe] are expected to be different for intrinsic and extrinsic stars with a likelihood that, if the mass transfer is not selective, extrinsic stars could show lower values than intrinsic stars of the same metallicity. Remarkably, the run (Figure 8) of [ls/Fe] versus [Fe/H] follows the theoretical prediction for ST/1.5 for intrinsic AGBs, while extrinsic ones lie on average below the curves, as expected. If the predictions were reduced by only about 0.2 dex, the fit would be even more satisfactory, especially for Galactic disk stars. This can easily be achieved, when one considers that model curves refer to the final AGB situation, while several intrinsic AGBs (MS, S stars) are certainly in a previous stage, and therefore have not yet reached the terminal values of their *s* enhancements (see later § 3.4, and also Abia et al. 2001). In light of Figure 3, a better average trend can alternatively be obtained by choosing a prediction between the ST/1.5 and ST/3 values. This possibility of accounting for the observed data by varying either the efficiency of nucleosynthesis or that of mixing was already encountered in Paper I, where we showed as sometimes only consideration of the whole distribution of *s* elements (if available) can solve this ambiguity. Observed and predicted [hs/Fe] indices are shown in Figure 9. Disk stars, especially for

$[\text{Fe}/\text{H}] > -0.5$ , fit the prediction for ST/1.5 reasonably well, as above. There is a hint that observations for the intrinsic stars fall below the ST/1.5 model curve around  $[\text{Fe}/\text{H}] \simeq -1$ , and the same duplicity of solutions mentioned for the ‘ls’ abundances applies.

In short, the collated observations of *s*-enrichment in intrinsic and extrinsic stars are, as a whole, rather well accounted for by the models of *s*-processing and TDUs in AGB stars. In particular, predictions for the ST/1.5 case provide, at all metallicities, a sort of average trend that nicely compares with observations, when the effects of mixing are taken into account. Our analysis considered a mass of  $1.5 M_{\odot}$  for the AGB star. In general this is not a critical choice; Figures 3 and 4 show a weak dependence of the predictions on initial stellar mass, as long as we consider low mass AGB stars. However, some exceptions exist. Four examples in Figure 7 have been mentioned. Three additional cases are HR 774, BD +75°348, and IRAS 07134+1005. We find a solution with  $3 M_{\odot}$  models in the first two cases, and we need a mass lower than  $1.5 M_{\odot}$  in the last one (see § 4, also for the peculiar case of HD 25329). Information on the initial mass of the AGB star is provided by detailed comparisons of observed abundances with theoretical predictions for  $[\text{hs}/\text{ls}]$ ,  $[\text{ls}/\text{Fe}]$ , and  $[\text{hs}/\text{Fe}]$ , as deduced by Figures 3a,b,c for  $M = 1.5 M_{\odot}$  and by Figures 4a,b,c for  $M = 3 M_{\odot}$ , respectively. Indeed, the values of these parameters provided by the models are rather sensitive to the initial mass (and to the metallicity) of the model star adopted.

### 3.4. A closer look at the role of mixing.

Concerning the two parameters (efficiency of mixing and of nucleosynthesis) that affect the *s*-process distributions of Figures 7 to 9, we actually have tools to discriminate their relative role thanks to the fact that models of the envelope abundances were computed pulse after pulse. An example of this is shown in Figure 10, which is the equivalent of Figure 2 of Paper I and Figure 6 of Paper II, but is computed with the new models: it is built for Galactic-disk metallicity models of  $1.5 M_{\odot}$  and contains only data points for Galactic-disk stars. The continuous lines show model envelope enrichments up to our last TDU episode, for different *s*-process efficiencies, as measured by the value of the number ratio between  $^{13}\text{C}$  and iron in the pocket. In order to understand the importance of gradual mixing, the dashed lines connect the points representing the 4th and 8th TDU episode. The figure shows clearly how many stars have abundances that are best explained by situations less extreme than those of Figures 3 and 4, which represent the termination points in the distributions of Figure 10. In particular, several MS/S stars with technetium in their spectra find a solution only with a limited number of TDU episodes, as expected by their belonging to a class intermediate between unprocessed M giants and C stars. A complementary view

is provided by Figures 11 and 12, where the curves (again from the  $1.5 M_{\odot}$  case) show model envelope compositions at different metallicities (similarly to Figure 3) in the plane  $[\text{s}/\text{Fe}]$  versus  $[\text{hs}/\text{ls}]$ . Here ‘s’ means the average of both ‘hs’ and ‘ls’ abundances and gives therefore integrated information on the  $s$ -element enrichment. The high non-linearity of the models as a function of the iron content of the star can be inferred by the indication on the plot of where the high and low metallicities lie. The loops correspond to the maxima in Figure 3. While Figure 11 represents the situation at the end of the AGB phase, Figure 12 is constructed with the predictions after only 4 pulses. This last case shows the composition of a material which is highly diluted, i.e. contains a small  $s$ -process enrichment from the He intershell. Most data points are bracketed by the predictions of the two plots, showing again that observations present to us a variety of mixing efficiencies. In these plots model curves allow one to appreciate only the total dilution, hence cannot discriminate between, for example, intrinsic MS stars and extrinsic Ba stars, though only the former class owes its dilution to an incomplete dredge up of He intershell material, while the second includes mass transfer in a binary system.

There are particular and intriguing issues in the plots from Figure 7 to Figure 12. Two will be mentioned: the case of the post-AGB stars and the Ba II stars, and the N-rich subdwarfs. As noted earlier (Reddy et al. 1999; Van Winckel & Reyniers 2000), there is a suggestion that the post-AGB intrinsic C-rich stars have a lower  $[\text{hs}/\text{ls}]$  than the Ba II giants. This difference of about 0.3 dex arises because of roughly equal and opposite offsets of the two groups in the indices  $[\text{ls}/\text{Fe}]$  and  $[\text{hs}/\text{Fe}]$ . Given that the atmospheres of the two groups of stars differ in temperature and surface gravity, the possibility exists that these small differences in  $[\text{ls}/\text{Fe}]$  and  $[\text{hs}/\text{Fe}]$  reflect systematic errors in the LTE analyses of either or both sets of stars. It is certainly premature to consider other explanations, among them selective accretion of elements by the extrinsic star in a mass transfer process. Detailed comparisons of observed and predicted abundances of Ba II giants could reveal clues to the possible difference with post-AGB stars; we discuss one such case in the next section. A further remarkable point to be mentioned for post-AGB stars is that our envelope compositions at the last thermal pulse found with the stellar code can fit them quite well, despite the noticeable envelope mass remaining in the models when TDU ceases. This may be a support to the finding that TDU disappears well before the envelope is completely eroded by mass loss. The physical reason has been suggested to lay in a sudden instability of the whole envelope, driven by a sharp reduction of the gas pressure and by the establishment of a super-Eddington luminosity (Lattanzio, Forestini, & Charbonnel 2000; Sweigart 1998; Wood & Faulkner 1986). A closer look at the N-rich subdwarf HD 25329 is given in the next section.

#### 4. Detailed photospheric compositions: a few examples

As mentioned in the previous subsection, consideration of just the hs and ls enhancements may leave unclear the relative importance of the two main processes controlling the abundances, i.e. the efficiency of neutron captures and the dilution mechanisms (firstly through TDU, subsequently through mass transfer, for the binary sources).

Disentangling the two effects is made easier when the detailed set of observations for individual elements is available, including the CNO group and other light nuclei. Indeed the synthesis of these last by the red giant is almost entirely unrelated to the efficiency of the neutron source. In particular, due to the rather fixed abundance of  $^{12}\text{C}$  in the He intershell at the occurrence of TDU ( $X(^{12}\text{C}) \simeq 0.20 - 0.23$ ) the photospheric abundance ratio between carbon and *s* elements helps to set independent constraints on the dilution with the envelope. One must however take into account the complications introduced by the possible activation of H-burning processes in the envelope, that can burn  $^{12}\text{C}$  and produce  $^{13}\text{C}$  and  $^{14}\text{N}$ . These are HBB, occurring in stars of intermediate mass (Lattanzio & Forestini 1999; Lattanzio, Forestini, & Charbonnel 2000) and CBP in stars of mass  $M \leq 2.3M_{\odot}$  (Gilroy 1989; Gilroy & Brown 1991; Charbonnel 1995; Wasserburg, Boothroyd, & Sackmann 1995; see also discussion in BGW99). In IMS, when HBB is at play, the ratio  $^{12}\text{C}/^{13}\text{C}$  decreases to its CNO equilibrium value of  $\sim 3.5$  and remains rather low even during the TP-AGB phase. Concerning CBP in LMS, it reduces the ratio  $^{12}\text{C}/^{13}\text{C}$  already during the red giant phase, and its effects depend on the initial mass. According to observations of giant stars in Galactic Clusters, this ratio is  $\sim 12$  for  $M = 1.5 M_{\odot}$ . It decreases to the CNO equilibrium value for giant stars of  $M \leq 1 M_{\odot}$  in Globular Clusters. During the AGB phase, it is possible for CBP to continue its operation, thus converting part of the primary  $^{12}\text{C}$  mixed with the envelope by TDU into  $^{14}\text{N}$  (Wasserburg, Boothroyd, & Sackmann 1995).

When our analysis is extended toward low metallicities, the task of reproducing carefully the abundance distributions of individual sources by operating such a dilution is complicated by the need to consider the possibly highly non-solar initial composition, characterized by a large scatter in the initial abundances of heavy nuclei. Here it is worth showing some examples, in order to demonstrate that, despite this, new pieces of information can be achieved on the mass and evolutionary status of the target stars.

We show therefore, in Figure 13, 14, 15, three examples of a thorough comparison between nucleosynthesis predictions and spectroscopic observations. For the sake of these examples, the initial abundances of the stellar envelopes have been scaled to the appropriate metallicity, following the already mentioned average trends of heavy element abundances in the Galaxy, published by Gratton & Sneden (1994).



The cases shown were chosen because of their heterogeneity (representing high, intermediate and low metallicities; including a Ba star (extrinsic AGB), a post-AGB supergiant and a suspected extrinsic dwarf; and belonging to the giant, supergiant, and dwarf luminosity classes, respectively). Their characteristics and detailed fits are discussed below.

#### 4.1. HR 774: a Ba II giant star in the Galactic disk

After the pioneering work by Warner (1965), a large number of studies considered the heavy element abundances in classical Ba II giants. HR 774 being very bright ( $m_v = 5.96$  according to Smith 1984), has been the object of several spectroscopic observations (Tomkin & Lambert 1979, 1983; Smith 1984). Smith (1984) emphasised the relatively low  $^{12}\text{C}/^{13}\text{C}$  ratio, a feature noticed in extrinsic AGB stars (in CH stars) by Wallerstein & Greenstein (1964). The set of observations adopted here is the one compiled in Paper II (Table 2) through averages of the various original observations. In particular we accept a metallicity  $[\text{Fe}/\text{H}] = -0.3 \pm 0.2$ . The data are modeled by generating the expected photospheric composition by dredging up carbon- and *s*-process-rich material from the He intershell to the envelope, according to the TDU efficiency of the stellar code, pulse after pulse. As shown in Figure 13, our best fit to the abundances comes from a binary system having a primary component of initially  $3 M_\odot$ , with a rather high efficiency in *s* processing (ST $\times$ 2), and a low mass secondary. In this example, the same results are obtained with two different mass transfer approaches. One assumes a single phenomenon of accretion, at the 20th TP, with a dilution of 0.2 (i.e. one part of the AGB envelope per 5 parts of the atmosphere of the secondary component). The second assumes a continuous process, up to the 20th pulse, and yields a dilution of 0.4. Due to the uncertainties on mass loss rates and our poor knowledge of how and when mass transfer phenomena occur, we do not claim that these are the only, or even the best solutions. They, however, indicate that a moderately massive primary component is necessary here. In this way we reach an agreement also for the carbon abundance, (values  $[\text{C}/\text{Fe}]$  in the range 0.5–0.7 can be obtained, depending on the assumptions made, to be compared with the observation  $0.7 \pm 0.1$ ). We found this datum difficult to reproduce otherwise.

#### 4.2. IRAS 07134+1005: a post-AGB supergiant

This star belongs to the group of supergiants showing the  $21 \mu\text{m}$  feature in their mid-infrared spectra, which is suspected to derive from C-rich compounds (Kwok, Volk, & Hrivnak 1989). Observations of molecular bands from CO, CN, HCN and  $\text{C}_2$  have been reported

by various authors (Bakker & Lambert 1998a,b; Bujarrabal, Alcolea, & Planesas 1992), so that both the C/O ratio and the  $^{12}\text{C}/^{13}\text{C}$  ratio are known. Optical spectroscopic observations of high precision were recently presented by Van Winckel & Reyniers (2000). They found it impossible to reproduce the measured *s*-element abundances with the parameterized calculations by Malaney (1987). The more complex *s*-process distributions of stellar models can instead perform this task, using cases of the appropriate metallicity ( $[\text{Fe}/\text{H}] = -1$ ). In the exercise shown in Figure 14, we found a good fit to the data with a  $1.5 M_{\odot}$  model with a relatively low efficiency in *s* processing (ST/3). With our choice for mass loss the fit requires 10 pulses; at this phase also the carbon and nitrogen enrichment are compatible with observations ( $[\text{C}/\text{Fe}] = 1.3$ ,  $[\text{N}/\text{Fe}] = 0.9$ , where observed values are  $1.1 \pm 0.1$  and  $0.85 \pm 0.15$ ). The suggested number of pulses is highly model dependent. Anyway, it indicates that the parent star was probably of initial mass lower than  $1.5 M_{\odot}$ , therefore experiencing only a limited number of TDU episodes.

#### 4.3. HD 25329: a star from an *s*-enriched cloud or a metal-poor Ba dwarf?

HD 25329 is currently classified as a halo dwarf, and is not particularly C rich, but very N rich. Beveridge & Sneden (1994) conclude that the star has a metallicity  $[\text{Fe}/\text{H}] = -1.8$  (possible uncertainty is of the order of  $\pm 0.2$  dex). These authors derived C, N, and O abundances as well as abundances of light, iron-peak, and heavy elements. Gay & Lambert (2000) showed that HD 25329 is marked by an apparently high abundance of the isotopes  $^{25}\text{Mg}$  and  $^{26}\text{Mg}$  relative to  $^{24}\text{Mg}$ . It shows  $^{26}\text{Mg}/^{24}\text{Mg} \simeq 0.09$ , where this ratio is 0.03 in the normal subdwarf HD 103095 of slightly higher metallicity.

Spectroscopic observations revealing enrichment in heavy elements were early presented by Peterson (1981a,b), who attributed them to explosive nucleosynthesis. Subsequently, Beveridge & Sneden (1994) obtained high S/N spectra from which they derived the abundances of *s* elements that we analyse here. These authors suspected that the enhancements of heavy nuclei might originate in the He-burning shell of an AGB star, but, as they could not confirm this star to be a spectroscopic binary, suggested that HD 25329 formed from gas polluted by ejecta from one or more AGB stars. The higher than expected abundance of  $^{25}\text{Mg}$  and  $^{26}\text{Mg}$  (relative to the normal abundance of  $^{24}\text{Mg}$ ) suggests that the ejecta came from intermediate mass AGB stars. Our attempts to fit the abundances of this *s*-enriched dwarf may confirm this conclusion (see below).

We addressed the problem through two exercises, whose results are shown in Figure 15. In the first attempt (lower panel), excluding for the moment Mg isotopes, we succeed in reproducing the observed *s*-process data within their uncertainties, as well as the relatively

low C abundance, by adopting a model of very low efficiency in neutron production (ST/12). The fit shown adopts an initial mass  $M = 1.5 M_{\odot}$ . The  $s$  element abundances must not grow too much in the AGB primary star, because the observed enhancements are rather small. This can be obtained, for example, if the primary component experiences only a limited number of TDU episodes (less than 10, as assumed in the Figure; this may be rather typical for these metallicities and also allows one to limit the carbon enrichment, which in our model is  $[C/Fe] = 0.5$ , against an observation of  $0.6 \pm 0.1$ ). A good fit to the  $s$  abundances can be obtained either with a unique mass transfer episode at the 8th TDU episode (yielding a dilution of 0.33, i.e. one part of the AGB envelope over three parts of the companion’s atmosphere) or with a continuous addition, lasting from the first to the eighth TDU episode (and in this case a larger fraction of the observed material would come from the AGB envelope, yielding a dilution of 0.54, due to the lower  $s$  enrichment in the first pulses). These details are however very model dependent. In this example the enhancements of N and  $^{25,26}\text{Mg}$  cannot be explained, and we would be forced to assume that these anomalies are inherited from the parent cloud. In a second exercise (upper panel) we showed that  $s$ -process abundances might also derive from a mass transfer episode from an IMS primary of initially  $5 M_{\odot}$ . This second exercise needs a noticeable  $^{13}\text{C}$  concentration in the pocket (for the assumptions in IMS and the definition of what is the ‘ST case’ there, see e.g. Travaglio et al. 2001). This solution is however not completely satisfactory for the light elements. Indeed, to reach the observed abundances, we have to assume that several pulses were made by the primary component, to compensate for the large dilution in the massive AGB envelope. This leads to a C-rich secondary ( $C/O > 1$ ), contrary to the observations. We might obviously assume that HBB burns this extra carbon (Lattanzio & Forestini 1999), but we did not apply a proper model to this. Also,  $^{26}\text{Mg}$  becomes too high, with a ratio  $^{26}\text{Mg}/^{24}\text{Mg}$  close to 0.3 for an initially solar Mg isotopic mix.

We therefore prefer the idea advanced by Beveridge & Sneden (1994), according to which this source might have formed from a natal cloud previously contaminated in  $s$ -process elements by a few AGBs, including at least one IMS. Unfortunately, our arguments are not strong enough to exclude completely the alternative hypothesis that it is a low-metallicity Ba dwarf, born with somewhat anomalous light element abundances. From Figure 15 we can however at least get a tool to discriminate the mass of the contaminating source(s). As shown by the two distributions, the requirements imposed by the other  $s$  elements yield in the two cases very different predictions for Pb, which is expected to be very high if IMS were at play here. We leave this tentative suggestion to future observational tests.

## 5. Conclusions

In this paper we have shown how present AGB modeling can satisfactorily account for the *s*-element enrichment observed at the surface of intrinsic and extrinsic AGB stars of different metallicities, from solar down to extreme halo composition. Agreement between model predictions and average observed abundances for heavy (Ba-peak group) and light (Zr-peak group) *s* elements (hs and ls) can be obtained by varying over a rather narrow interval the abundance of  $^{13}\text{C}$  burnt per nucleosynthesis episode. The almost linear relationship between the neutron-flux sensitive parameter [hs/ls] and [Fe/H], which roughly holds at Galactic disk metallicities, breaks down for halo stars. The reason for this is primarily that at very low [Fe/H] values the number of neutrons captured by iron seeds and their progeny becomes so large that the *s*-process path is followed to its end at  $^{208}\text{Pb}$  (and at a lower extent at  $^{209}\text{Bi}$ ). The [hs/ls] parameter grows with the total *s* enrichment [s/Fe] in the envelope, with a functional relationship that appears roughly linear for post-AGB stars (as noticed by Van Winckel & Reyniers 2000), but in reality displays a loop-like trend and is different for AGB and post-AGB stars, reflecting different dilution factors of the *s*-processed matter with the envelope. We also showed how the models can account for the detailed distributions of *s*-elements and for the abundance of CNO nuclei, when they are available, and how this type of comparisons can add new pieces of information concerning the initial mass, the number of thermal pulses occurred and the dilution efficiency for extrinsic AGB stars.

This work was supported by MURST through the grant COFIN2000–Evoluzione Stellare, the U.S. NSF through grants to DLL (grant AST96-18414) and to VVS (grant AST96-18459), and the Robert A. Welch Foundation. We are deeply indebted to O. Straniero, A. Chieffi and M. Limongi for their longstanding fundamental collaboration in stellar modeling. We are also grateful to the referee, Beatriz Barbuy, for her helpful and constructive comments.

## REFERENCES

- Abia, C., & Wallerstein, G. 1998, *MNRAS*, 293, 89
- Abia, C., Busso, M., Gallino, R., Dominguez, I., & Straniero, O. 2001, *ApJ*, (submitted)
- Anders, E., & Grevesse, N. 1989, *Geochim. Cosmochim. Acta*, 53, 197
- Aoki, W., Norris, J.E., Ryan, S.G., Beers, T.C., & Ando, H. 2000, *ApJ*, 536, L97

- Arlandini, C., Käppeler, F., Wisshak, K., Gallino, R., Lugaro, M., Busso, M., & Straniero, O. 1999, *ApJ*, 525, 886
- Asplund, M., Gustafsson, B., Lambert, D.L., & Rao, N.K. 2000, *A&A*, 353, 287
- Asplund, M., Lambert, D.L., Kipper, T., Pollacco, D., & Shetrone, M.D. 1999, *A&A*, 343, 507
- Bakker, E.J., & Lambert, D.L. 1998a, *ApJ*, 502, 417
- Bakker, E.J., & Lambert, D.L. 1998b, *ApJ*, 508, 387
- Barbuy, B., Cayrel, R., Spite, M., Beers, T.C., Spite, F., Nordström, B., Nissen, B.E. 1997, *A&A*, 317, L63
- Bessell, M.S., & Norris, J.E. 1982, *ApJ*, 263, L29
- Beveridge, R.C., & Sneden, C. 1994, *AJ*, 108, 285
- Blanco, V.M., McCarthy, M.F., & Blanco, B.M. 1980, *ApJ*, 242, 938
- Boothroyd, A., & Sackmann, I.-J. 1988, *ApJ*, 328, 671
- Boothroyd, A., & Sackmann, I.-J. 1999, *ApJ*, 510, 232
- Bujarrabal, V., Alcolea, J., & Planesas, P. 1992, *A&A*, 257, 701
- Burris, D.L., Pilachowski, C.A., Armandroff, T.E., Sneden, C., Cowan, J.J., Roe, H. 2000, *ApJ*, 544, 302
- Busso, M., & Gallino, R. 1997, *Nucl. Phys.*, A621, 431c
- Busso, M., Gallino, R., Lambert, D.L., Raiteri, C.M., & Smith, V.V. 1992, *ApJ*, 399, 218 (Paper I)
- Busso, M., Gallino, R., & Wasserburg, G.J. 1999, *ARA&A*, 37, 239 (BGW99)
- Busso, M., Lambert, D.L., Beglio, L., Gallino, R., Raiteri, C.M., & Smith, V.V. 1995, *ApJ*, 446, 775 (Paper II)
- Busso, M., Picchio, G., Gallino, R., & Chieffi, A. 1988, *ApJ*, 326, 196
- Cayrel, R., Hill, V., Beers, T.C., Barbuy, B., Spite, M., Spite, F., Plez, B., Andersen, J., Bonifacio, P., Francois, P., Molaro, P., Nordström, B., & Primas, F. 2001, *Nature*, 409, 691

- Charbonnel, C. 1995, *ApJ*, 453, L41
- Charbonnel, C., Brown, J.A., & Wallerstein, G. 1998, *A&A*, 332, 204
- Clayton, D.D. 1988, *MNRAS*, 234, 1
- Clayton, D.D., & Rassbach, M.E. 1967, *ApJ*, 168, 69
- Clegg, R.E.S., Lambert, D.L., & Bell, R.A. 1979, *ApJ*, 234, 188
- Cristallo, S., Gallino, R., Straniero, O., Lugaro, M., & Busso, M. 2001, *Nuclear Phys. A.*, in press
- Denker, A., Drotleff, H.W., Grosse, M., Knee, H., Kunz, R., et al. 1995, in *Nuclei in the Cosmos III*, ed. M. Busso, R. Gallino, C.M. Raiteri (New York: AIP), 255
- Edvardsson, B., Andersen, J., Gustafsson, B., Lambert, D.L., Nissen, P.E., & Tomkin, J. 1993, *ApJ*, 275, 101
- Frost, C.A., Cannon, R.C., Lattanzio, J.C., Wood, P.R., & Forestini, M. 1998, *A&A* 332, L17
- Frost, C.A., Lattanzio, J.C., & Wood, P.R. 1998, *ApJ*500, 355
- Gallino, R., Arlandini, A., Busso, M., Lugaro, M., Travaglio, C., Straniero, O., Chieffi, A., & Limongi, M. 1998, *ApJ*, 497, 388 (G98)
- Gallino, R., Busso, M., Picchio, G., Raiteri, C.M., & Renzini, A. 1988, *ApJ*, 334, L45
- Gay, P.L., & Lambert, D.L. 2000, *ApJ*, 533, 260
- Gilroy, K.K. 1989, *ApJ*, 347, 835
- Gilroy, K.K., & Brown, J.A. 1991, *ApJ*, 371, 578
- Goriely, S., & Mowlavi, N. 2000, *A&A* 599, 614
- Gonzalez, G., Lambert, D.L., Wallerstein, G., Rao, N.K., & Smith, V.V. 1997, *ApJS*, 114, 133
- Gratton, R.G., & Sneden, C. 1994, *A&A*, 287, 927
- Han, Z., Eggleton, P.P., Podsiadlowski, P., & Tout, C.A. 1995, *MNRAS*, 277, 1443
- Herwig, F. 2000, *A&A*, 360, 952

- Herwig, F., Blöcker, T., Schönberner, D., & El Eid, M. 1997, *A&A*, 324, L81
- Herwig, F., Schönberner, D., Blöcker, T. 1998, *A&A*, 339, 123
- Hill, V, Barbuy, B., Spite, M., Spite, F., Cayrel, R., Plez, B., Beers, T.C., Nordström, B., Nissen, B.E. 2000, *A&A*, 353, 557
- Hill, V., Plez, B., Cayrel, R., & Beers, T.C. 2001 (preprint)
- Hollowell, D.E., & Iben, I. Jr 1988, *ApJ*, 333, L25
- Iben, I. Jr 1975, *ApJ*, 196, 525
- Iben, I. Jr, & Renzini, A. 1982, *ApJ*, 263, L23
- Iben, I. Jr, & Renzini, A. 1983, *ARA&A*, 21, 271
- Jorissen, A., & Mayor, M. 1988, *A&A*, 198, 187
- Jorissen, A., Van Eck, S., Mayor, M., & Udry, S. 1998, *A&A*, 332, 877
- Käppeler, F., Beer, H., & Wisshak, K. 1989, *Rep. Progr. Phys.*, 52, 945
- Käppeler, F., Gallino, R., Busso, M., Picchio, G., & Raiteri, C.M. 1990, *ApJ*, 354, 630
- Kipper, T. 1992, *Baltic Astr.*, 1, 181
- Kipper, T., & Jørgensen, U.G. 1994, *A&A*, 290, 148
- Kipper, T., Jørgensen, U.G., Klochkova, V.G., & Panchuk, V.E. 1996, *A&A*, 306, 489
- Kipper, T., & Kipper, M. 1990, *Sov. Astron. Lett.*, 16, 478
- Kovács, R.L. 1985, *A&A*, 150, 232
- Kwok, S., Volk, K.M., & Hrivnak, B.J. 1989, *ApJ*, 345, 51
- Lambert, D.L. 1985, in *Cool Stars with Excesses of Heavy Elements*, ed. M. Jaschek & P.C. Keenan (Dordrecht: Reidel), 191
- Lambert, D.L., Smith, V.V., Busso, M., Gallino, R., & Straniero, O. 1995, *ApJ*, 450, 302
- Langer, N., Heger, A., Wellstein, S., & Herwig, F. 1999, *A&A*, 346, L37
- Lattanzio, J.C., & Forestini, M. 1999, in *Asymptotic Giant Branch Stars*, IAU Symp. 191, ed. T. Le Bertre, A. Lèbre, & C. Waelkens (San Francisco: IAU Publ.), 447

- Lattanzio, J.C., Forestini, M., & Charbonnel, C. 2000, in *The Changes in Abundances in Asymptotic Giant Branch Stars*, ed. F. D'Antona & R. Gallino, *Mem. Soc. Astron. It.*, in press
- Lattanzio, J.C., & Karakas, A.I. 2001, in *Salting the Early Soup: Trace Nuclei from Stars to the Solar System*, ed. M. Busso & R. Gallino, *Mem. Soc. Astron. It.*, in press
- Luck, R.E., & Bond, H.E. 1984, *ApJ*, 279, 729
- Luck, R.E., & Bond, H.E. 1985, *ApJ*, 292, 559
- Luck, R.E., & Bond, H.E. 1991a, *ApJS*, 77, 515
- Luck, R.E., & Bond, H.E. 1991b, *ApJ*, 244, 919
- Luck, R.E., Bond, H.E., & Lambert, D.L. 1990, *ApJ*, 357, 188
- Malaney, R.A. 1987, *Ap&SS*, 137, 251
- McClure, R.D. 1983, *ApJ*, 268, 264
- McClure, R.D. 1984, *ApJ*, 280, L31
- McWilliam, A. 1997, *ARA&A*, 35, 503
- McWilliam, A. 1998, *AJ*, 115, 1640
- McWilliam, A., & Lambert, D.L. 1988, *MNRAS*, 230, 573
- McWilliam, A., Preston, G.W., Sneden, C., & Searle, L. 1995, *AJ*, 109, 2757
- McWilliam, A., Preston, G.W., Sneden, C., Searle, L., & Shectman, S. 1996, in *Formation of the Galactic Halo. Inside and Out*, ASP Conf. Series 92, ed. H. Morrison & A. Sarajedini (San Francisco: ASP), 317
- Merrill, P.W. 1952, *Science*, 115, 484
- Mowlavi, N. 1999, *A&A*, 350, 73
- Mowlavi, N., & Meynet, G. 2000, *A&A*, 361, 959
- Norris, J.E., Ryan, S.G., & Beers, T.C. 1997, *ApJ*, 488, 350
- Pereira, C.B., Smith, V.V., & Cunha, K. 1998, *AJ*, 116, 1997
- Peterson, R. C. 1981a, *ApJ*, 244, 989



- Peterson, R. C. 1981b, *ApJS*, 45, 421
- Plez, B., Smith, V.V., & Lambert, D.L. 1993, *ApJ*, 418, 812
- Qian, Y.-Z., & Wasserburg, G.J. 2001, *ApJ*, (in press)
- Qian, Y.-Z., Vogel, P., & Wasserburg, G.J. 1998, *ApJ*, 494, 285
- Reddy, B.E., Bakker, E.J., & Hrivnak, B.J. 1999, *ApJ*, 524, 831
- Reimers, D. 1975, in *Problems in Stellar Atmospheres and Envelopes*, ed. B. Baschek, H. Kegel, & G. Traving (Berlin: Springer), 229
- Ryan, S.G., Aoki, W., Blake, L.A.J., Norris, J.E., Beers, T.C., Gallino, R., Busso, M., & Ando, H. 2001, in *Salting the Early Soup: Trace Nuclei from Stars to the Solar System*, ed. M. Busso & R. Gallino, *Mem. Soc. Astron. It.*, in press
- Ryan, S.G., Norris, J.E., & Beers, T.C. 1996, *ApJ*, 471, 254
- Seeger, P.A., Fowler, W.A., & Clayton, D.D. 1965, *ApJS*, 11, 121
- Smith, V.V. 1984, *A&A*, 132, 326
- Smith, V.V., Coleman, H., & Lambert, D.L. 1993, *ApJ*, 417, 287
- Smith, V.V., Cunha, K., Jorissen, A., & Boffin, H.M.J. 1996, *A&A*, 315, 179
- Smith, V.V., Cunha, K., Jorissen, A., & Boffin, H.M.J. 1997, *A&A*, 324, 97
- Smith, V.V., & Lambert, D.L. 1984, *PASP*, 96, 226
- Smith, V.V., & Lambert, D.L. 1985, *ApJ*, 294, 326 (SL85)
- Smith, V.V., & Lambert, D.L. 1986, *ApJ*, 311, 843 (SL86)
- Smith, V.V., & Lambert, D.L. 1990, *ApJS*, 72, 387 (SL90)
- Smith, V.V., & Suntzeff, N.B. 1987, *AJ*, 93, 359
- Smith, V.V., Suntzeff, N.B., Cunha, K., Gallino, R., Busso, M., Lambert, D.L., & Straniero, O. 2000, *AJ*, 119, 1239
- Snedden, C., McWilliam, A., Preston, G.W., Cowan, J.J., Burris, D.L., & Armosky, B.J. 1996, *ApJ*, 467, 819

- Snedden, C., Cowan, J.J., Ivans, I.I., Fuller, G.M., Burles, S., Beers, T.C., Lawler, J.E. 2000, *ApJ*, 533, L139
- Straniero, O., Chieffi, A., Limongi, M., Busso, M., Gallino, R., & Arlandini, A. 1997, *ApJ*, 478, 332
- Straniero, O., Gallino, R., Busso, M., Chieffi, A., & Raiteri, C.M. 1995, *ApJ*, 440, L85
- Sweigart, A.V. 1998, in *New Views of the Magellanic Clouds*, IAU Symp. 190, ed. Y.-H. Chu, N. Suntzeff, J. Hesser, & D. Bohlender (San Francisco, IAU Publ.), 1370
- Tech, J.L. 1971, *Natl. Bur. Std. US. Monograph No. 119*
- Tomkin, J., & Lambert, D.L. 1979, *ApJ*, 227, 209
- Tomkin, J., & Lambert, D.L. 1983, *ApJ*, 273, 722
- Tomkin, J., & Lambert, D.L. 1986, *ApJ*, 311, 819
- Tomkin, J., & Lambert, D.L. 1999, *ApJ*, 523, 234
- Travaglio, C., Galli, D., Gallino, R., Busso, M., Ferrini, F., & Straniero, O. 1999, *ApJ*, 521, 691 (T99)
- Travaglio, C., Gallino, R., Busso, M., & Gratton, R.G. 2001, *ApJ*, 549, 346
- Truran, J.W., & Iben, I. Jr 1977, *ApJ*, 216, 797
- Ulrich, R.K. 1973, in *Explosive Nucleosynthesis*, ed. D.N. Schramm & W.D. Arnett (Austin: Univ. Texas Press), 139
- Vanture, A.D. 1992, *AJ*, 104, 1997
- Van Winckel, H., & Reyniers, C. 2000, *A&A*, 354, 135
- Wallerstein, G., & Greenstein, J.L. 1964, *ApJ*, 139, 1163
- Warner, B. 1965, *ApJ*, 221, 627
- Wasserburg, G.J., Boothroyd, A.I., & Sackmann, I.-J. 1995, *ApJ*, 447, L37
- Wasserburg, G.J., & Qian, Y.-Z. 2000, *ApJ*, 529, L21
- Westin, J., Sneden, C., Gustafsson, B., Cowan, J.J. 2000, *ApJ*, 530, 783
- Wood, P.R., Faulkner, D.J. 1986, *ApJ*, 307, 659

Začs, L., Klochkova, V.G., & Panchuk, V.E. 1995, MNRAS, 275, 764

Začs, L., Nissen, P.E., & Schuster, W.J. 1998, A&A, 337, 216

Začs, L., Schmidt, M.R., & Schuster, W.J., 2000, A&A, 358, 1022

Zhao, G., & Magain, P. 1991, A&A, 244, 425

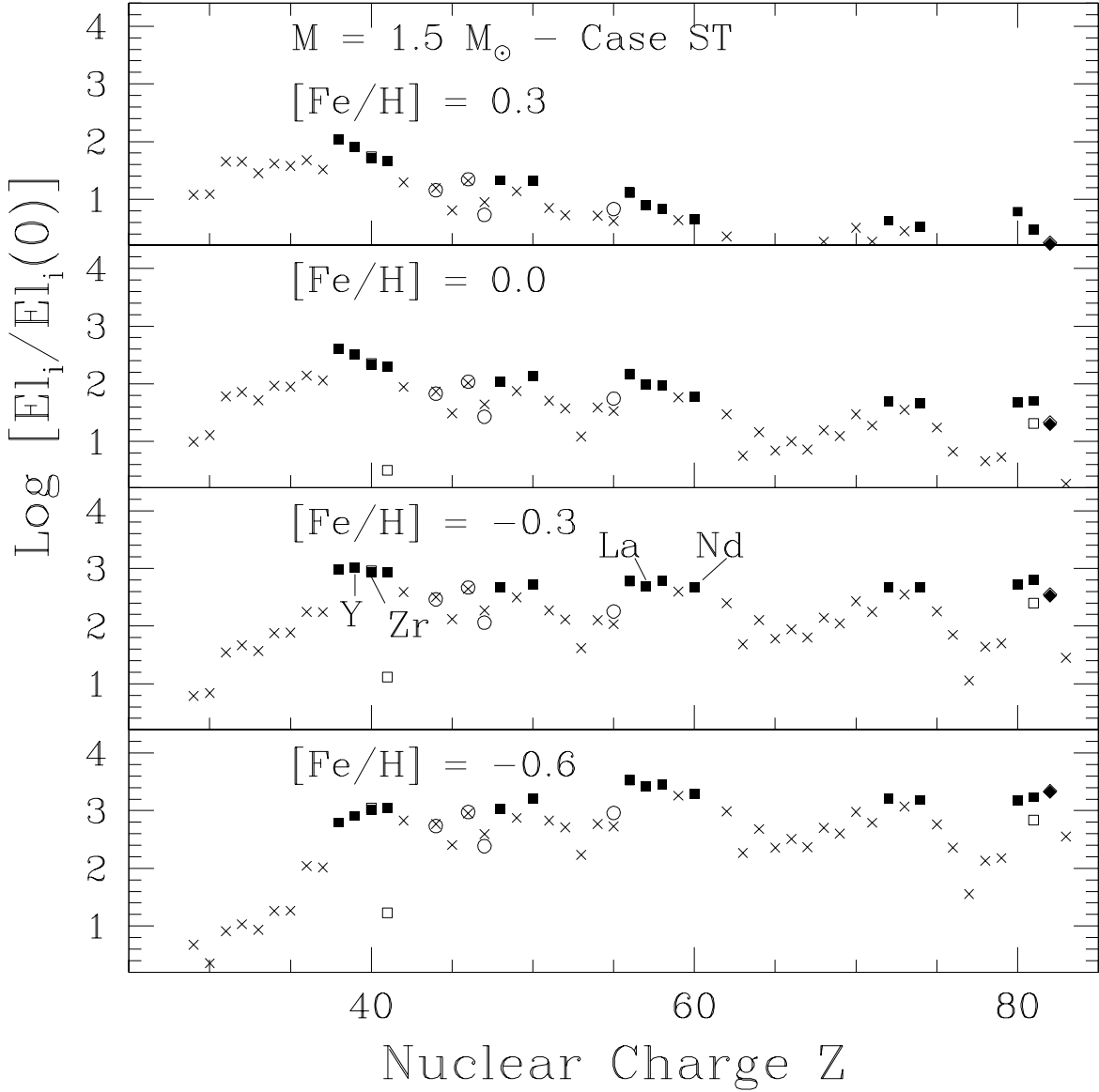


Fig. 1.— The distribution of the elements from Cu to Bi in the He intershell as a function of the initial metallicity. Elements mainly produced by the main component of the  $s$  process (by at least 50 % according to Arlandini et al. 1999) are shown as bold squares. Pb has a special symbol (bold diamond) because it is mainly attributed to the strong  $s$ -process component, deriving from AGB stars of low metallicity (Travaglio et al. 2001). The models refer to a  $1.5 M_{\odot}$  star, with the choice ST for the  $^{13}\text{C}$  pocket discussed in the text, and with metallicities from  $[Fe/H] = +0.3$  down to  $-0.6$ . For elements affected by the decay of unstable isotopes whose half-life is longer than a typical interpulse period, but shorter than  $10^9$  yr, open symbols refer to abundances before decay.

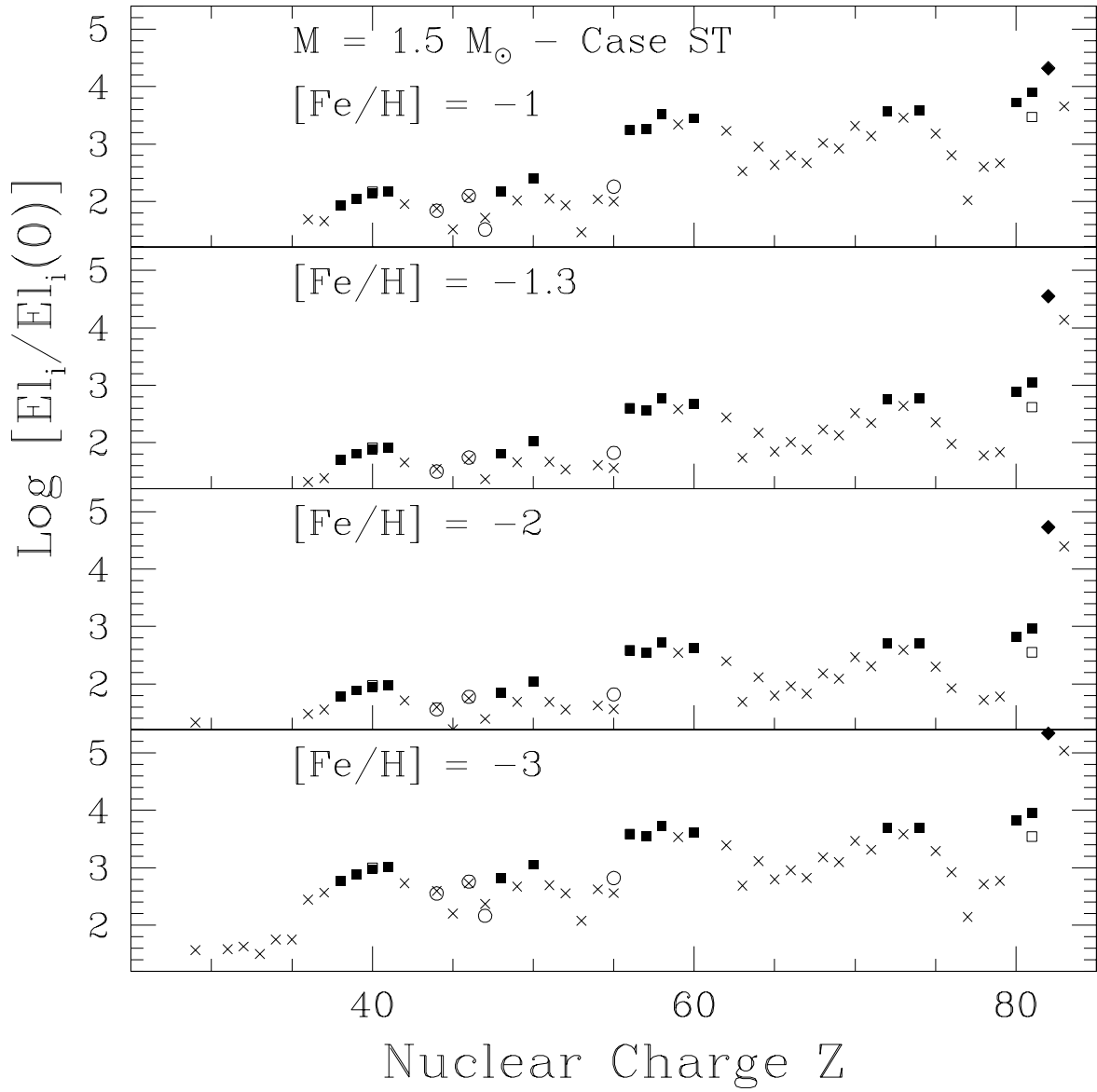
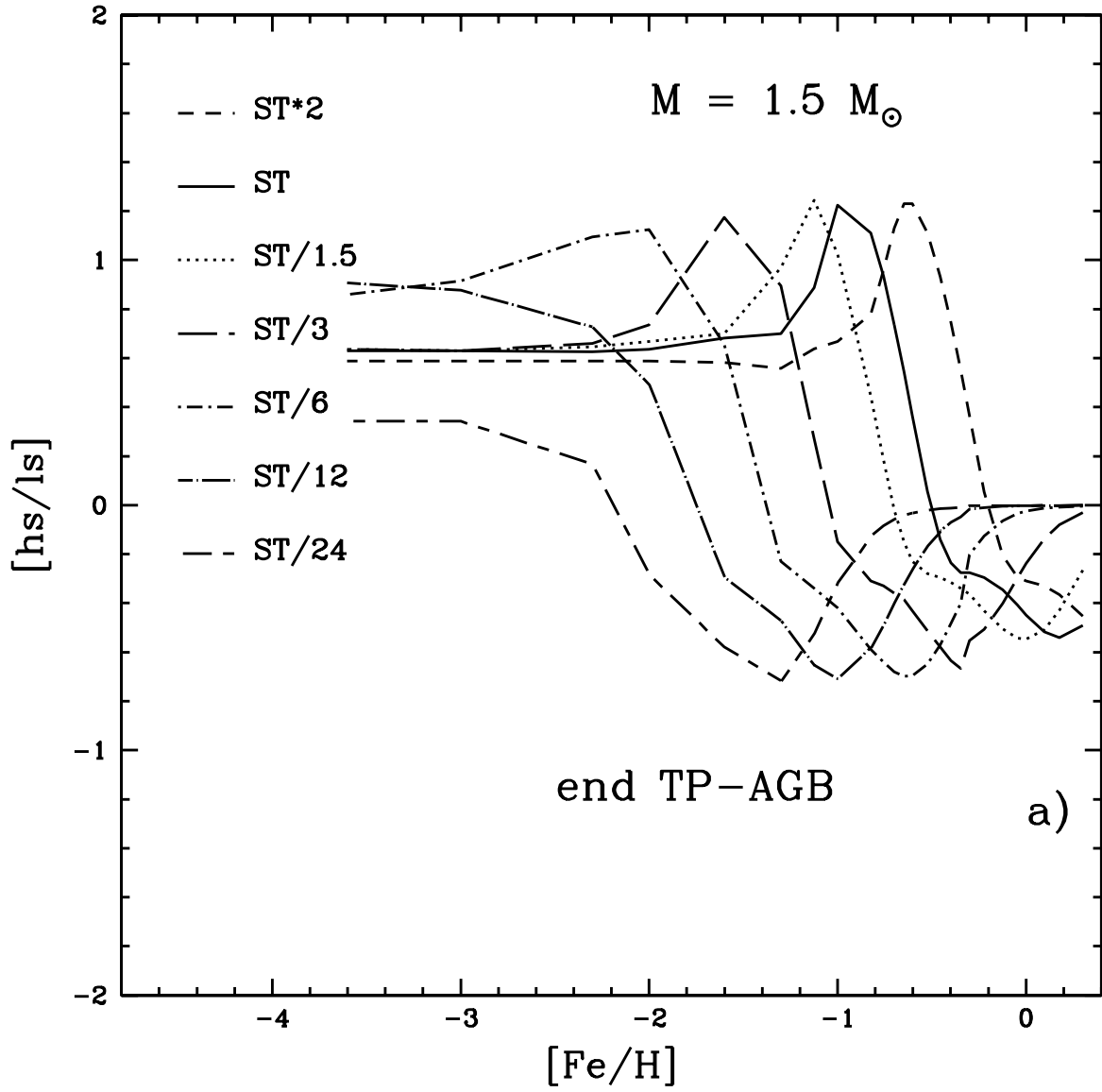
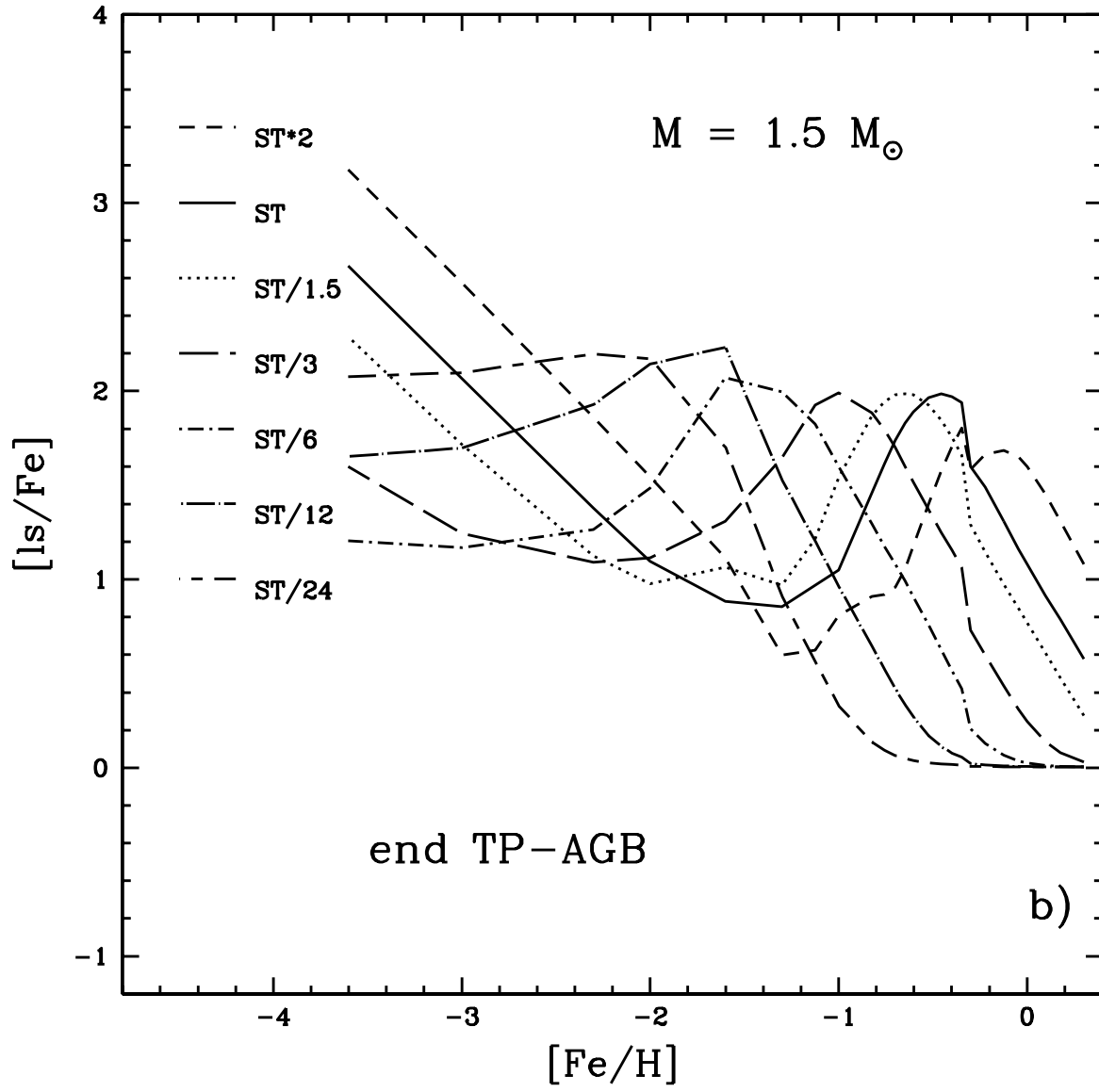


Fig. 2.— Same as Figure 1, but for metallicities from  $[\text{Fe}/\text{H}] = -1$  down to  $[\text{Fe}/\text{H}] = -3$ .





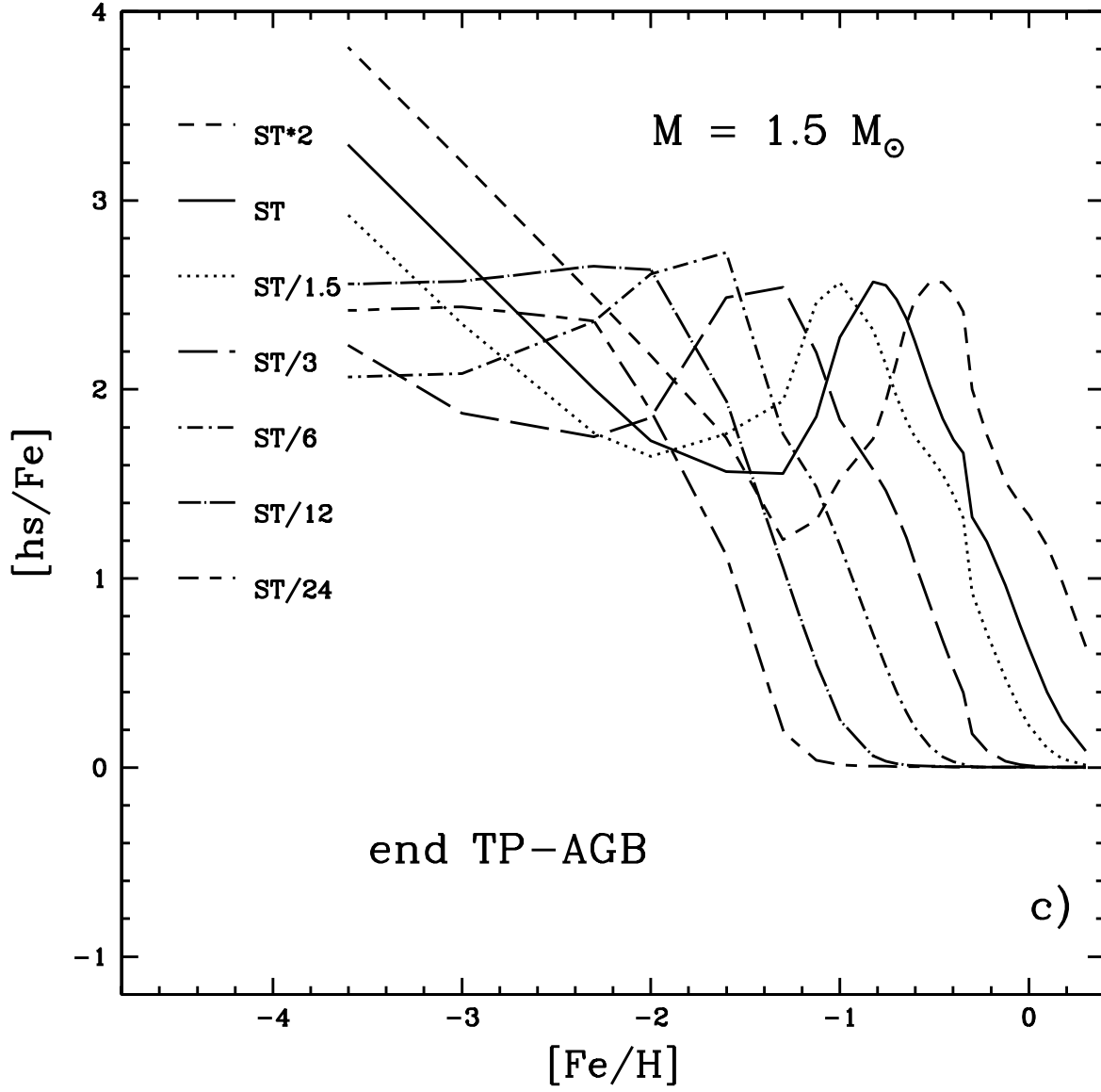
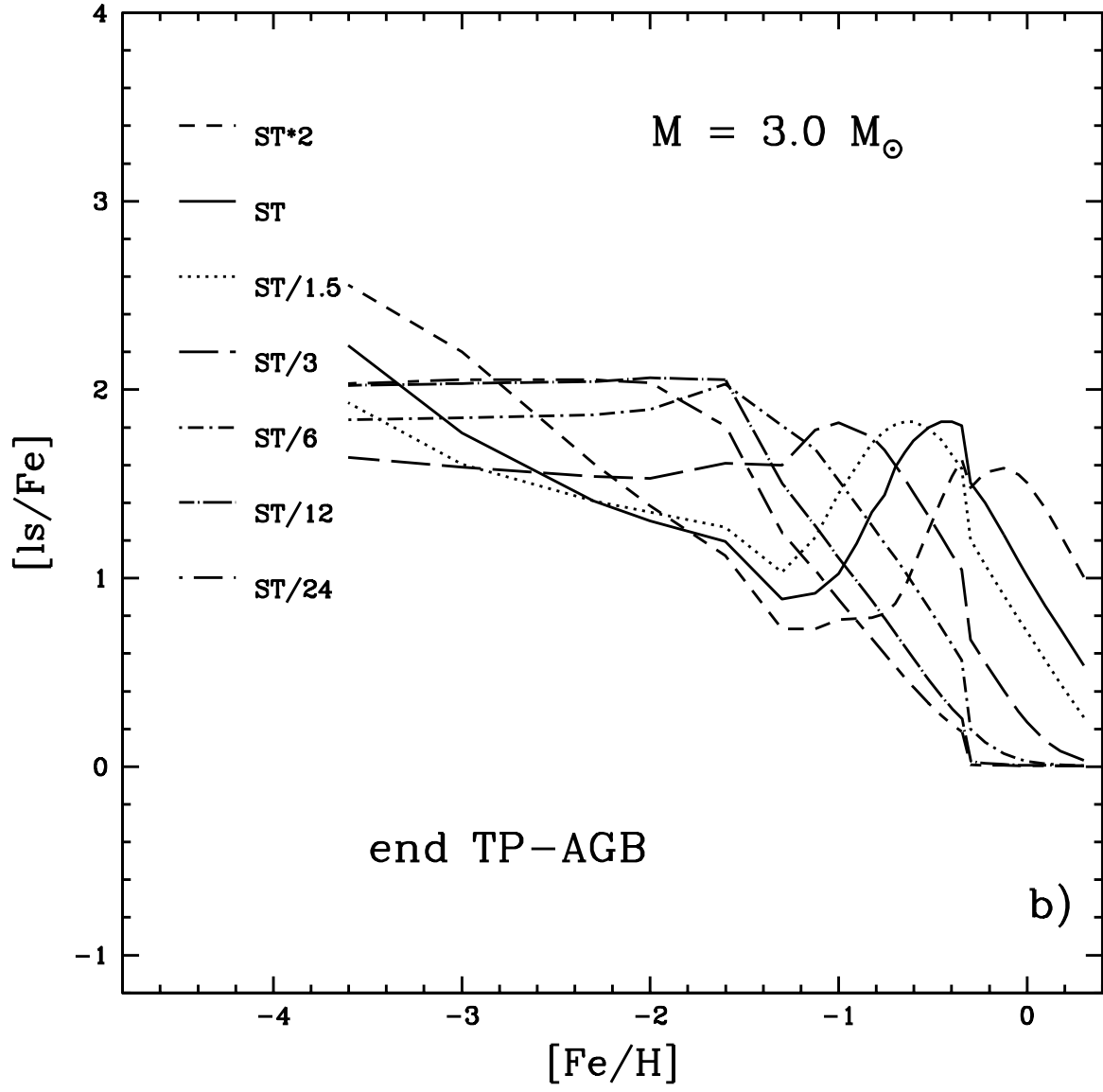


Fig. 3.— (a, b, c). Predicted ratios  $[hs/ls]$  (a),  $[ls/Fe]$  (b), and  $[hs/Fe]$  (c), from AGB stellar models of  $1.5 M_{\odot}$ . Each curve refers to a different choice of the  $^{13}\text{C}$  pocket, as shown by the labels and discussed in the text.







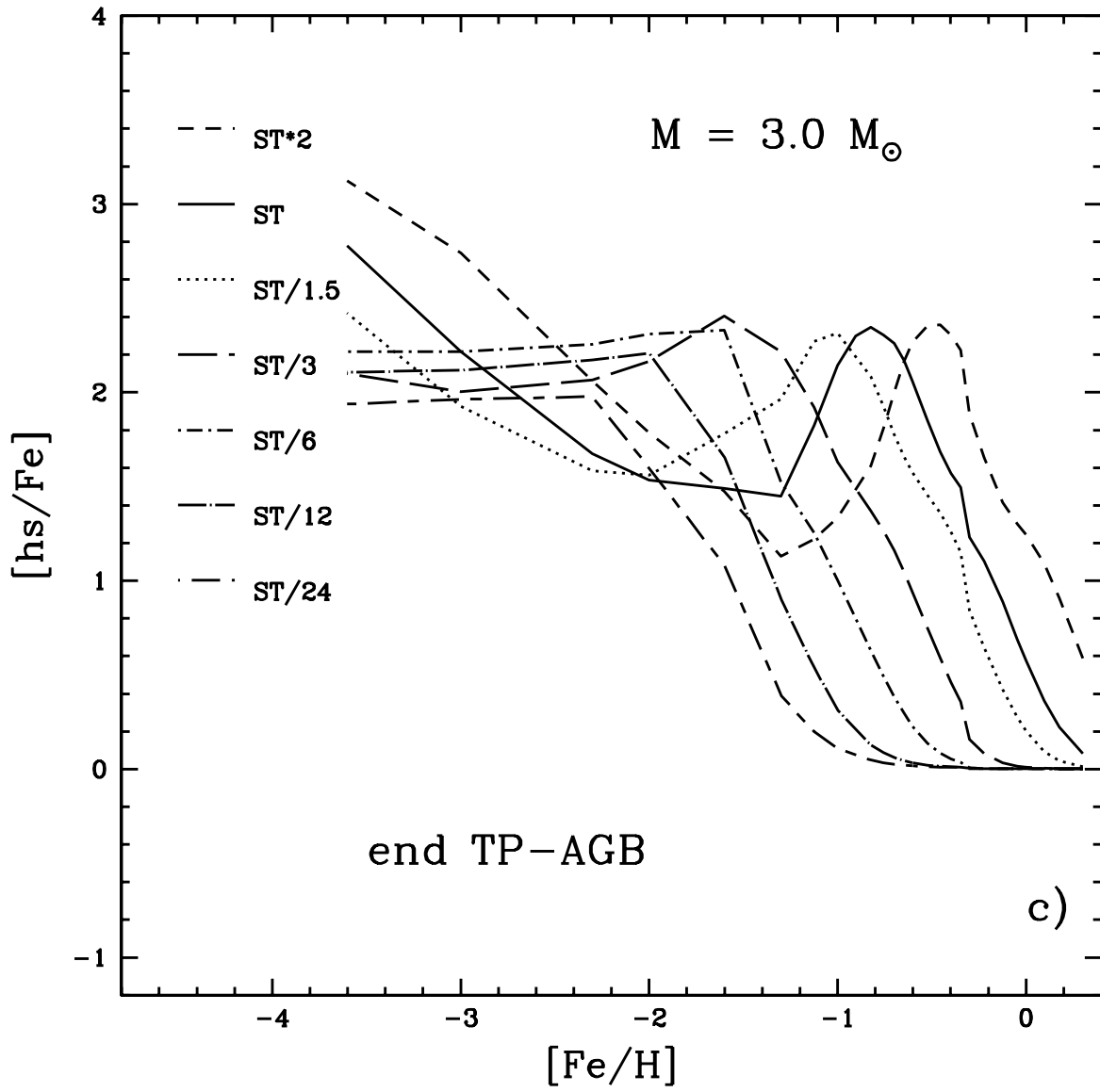


Fig. 4.— (a, b, c). Same as Figure 3, but for 3  $M_{\odot}$  stellar models.

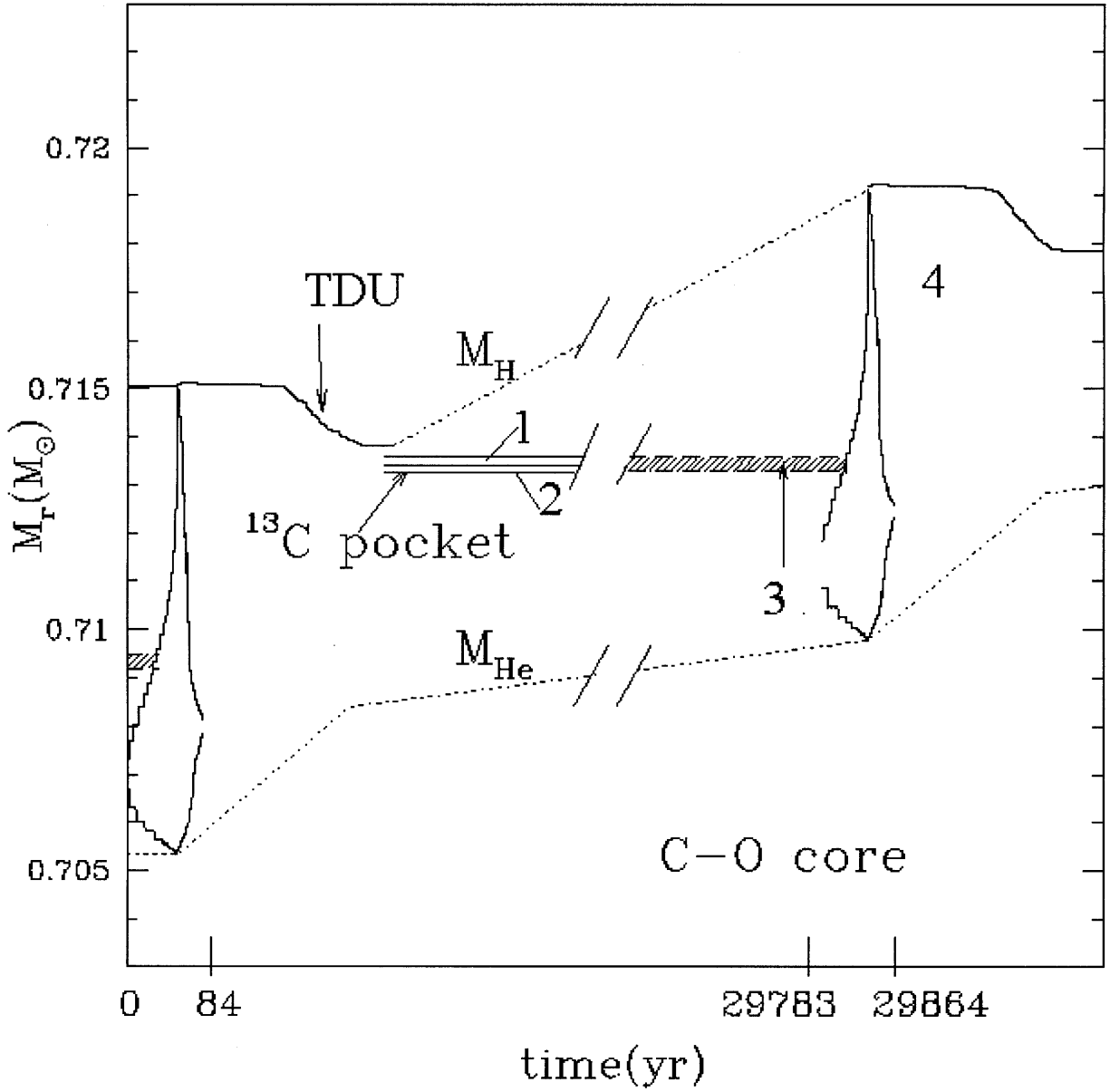


Fig. 5.— A sketch of the He-intershell structure through the development of two subsequent thermal pulses, showing the region where the  $^{13}\text{C}$  pocket forms. The zones relevant for understanding the results listed in Table 1 are indicated.

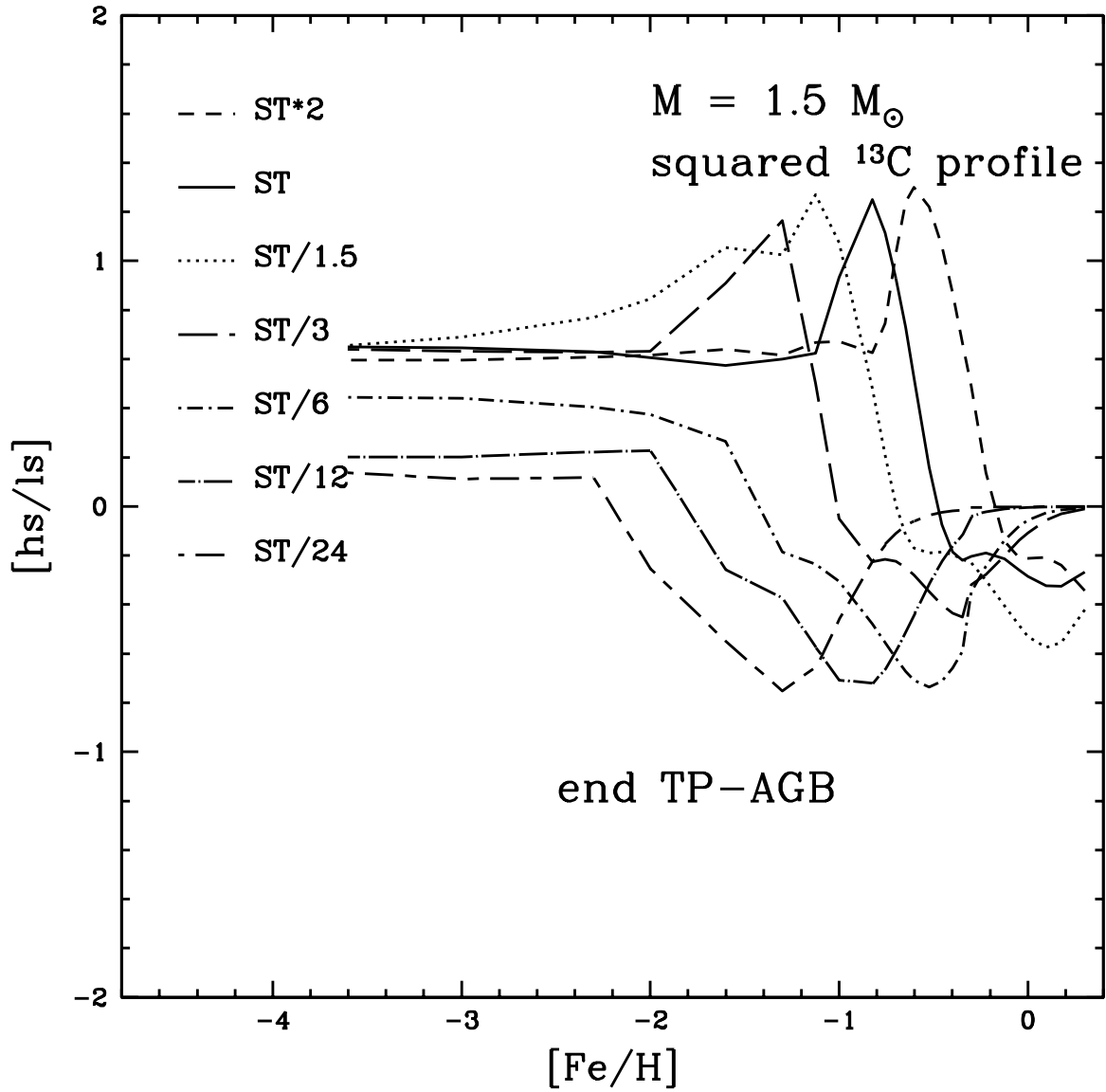


Fig. 6.— Predicted  $[\text{hs}/\text{ls}]$  ratios by AGB stellar models of  $1.5 M_{\odot}$  versus  $[\text{Fe}/\text{H}]$  for a flat  $^{13}\text{C}$  profile in the pocket, as discussed in the text.

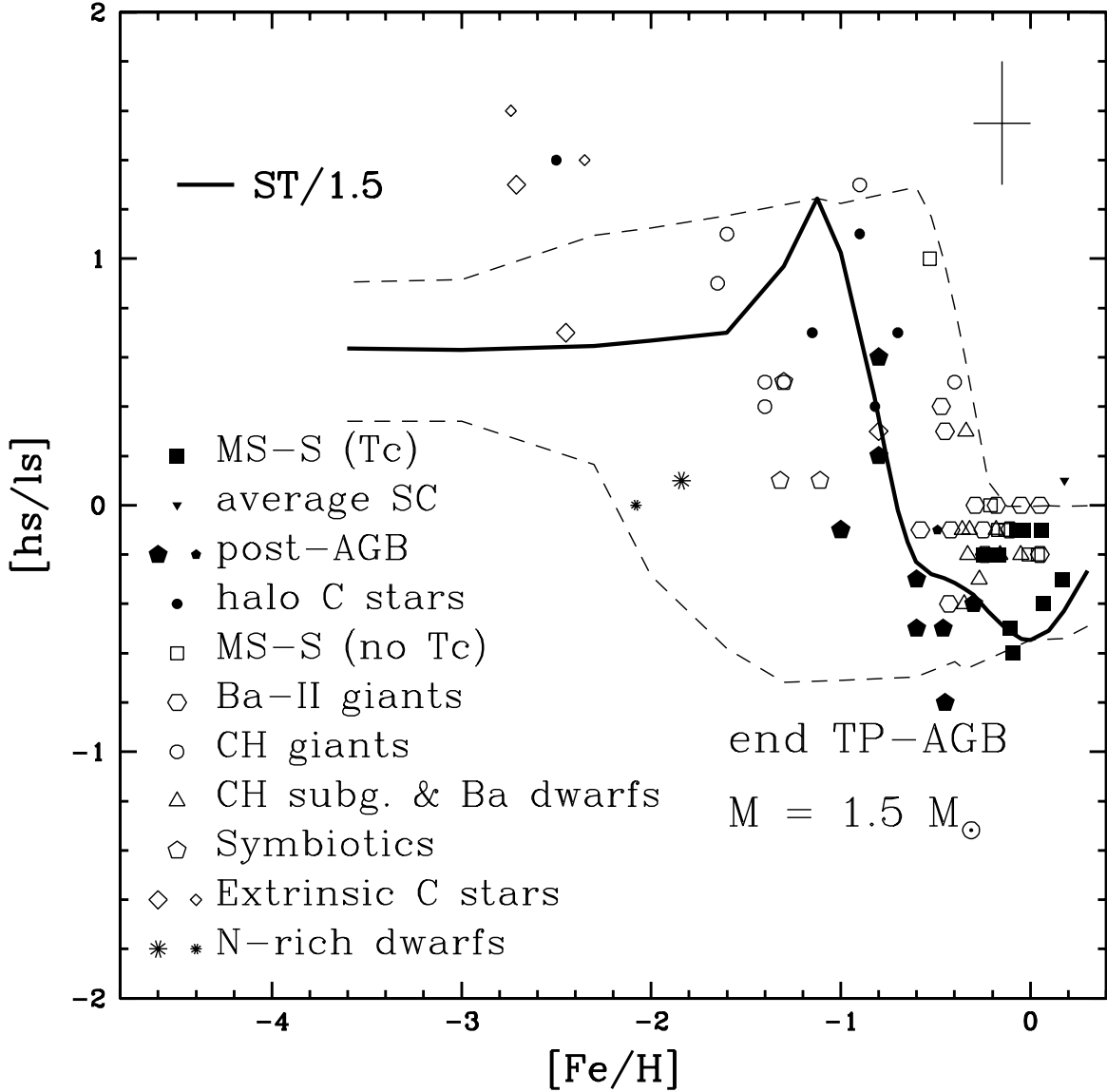


Fig. 7.— Observed abundance ratios  $[hs/lis]$  in the chosen set of intrinsic and extrinsic AGB stars at all metallicities. Filled and unfilled symbols refer to intrinsic and extrinsic stars, respectively. The typical value of the observational uncertainty is shown. SC stars have been represented by their average (see Table 2a). Small symbols refer to stars that have lower weight in our analysis, as explained in the text. Curves represent the predictions from the models specified on the figure itself.

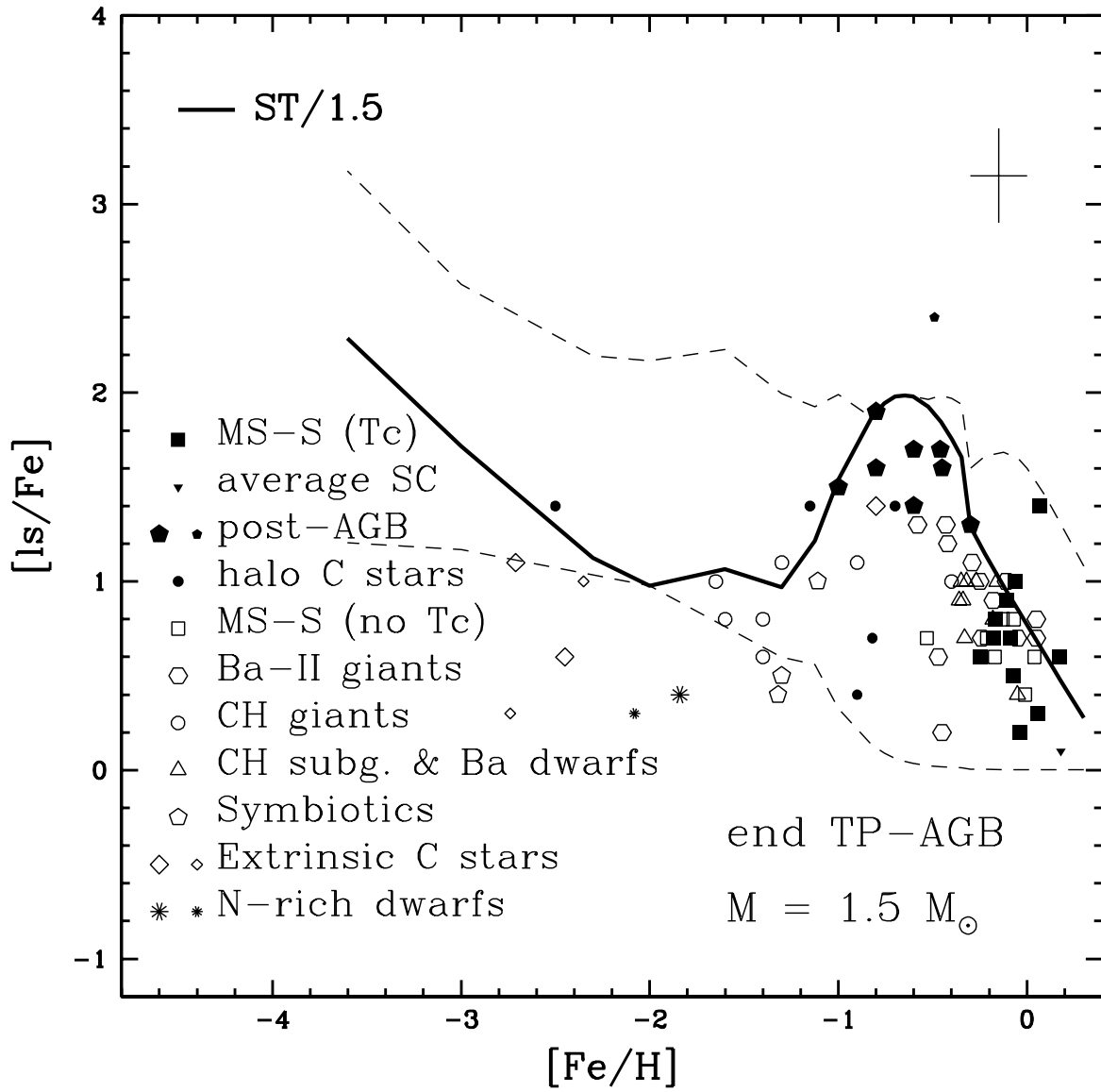


Fig. 8.— Same as Figure 7, for the  $[ls/Fe]$  abundance ratios.

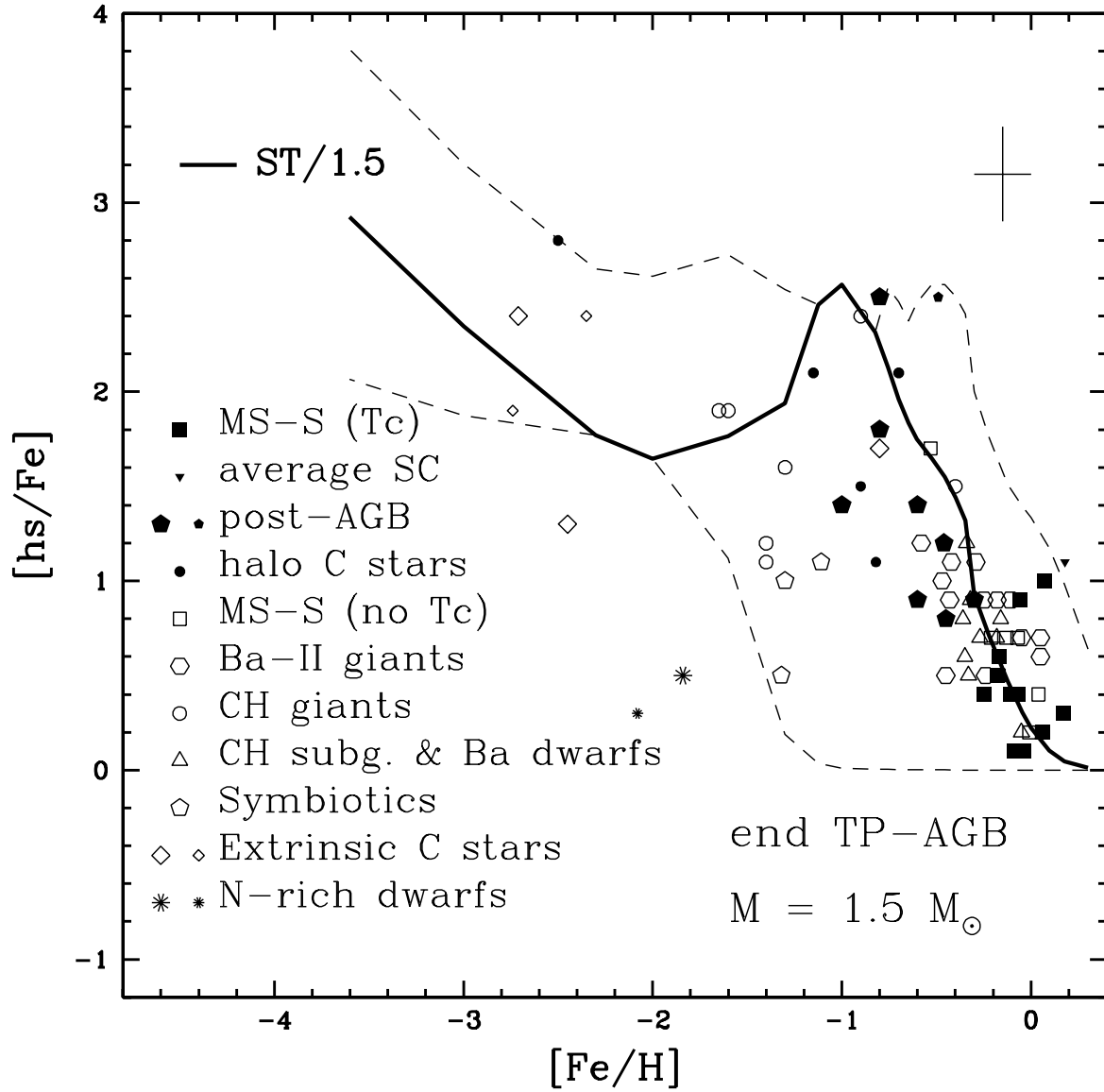


Fig. 9.— Same as Figure 7, for the  $[hs/Fe]$  abundance ratios.



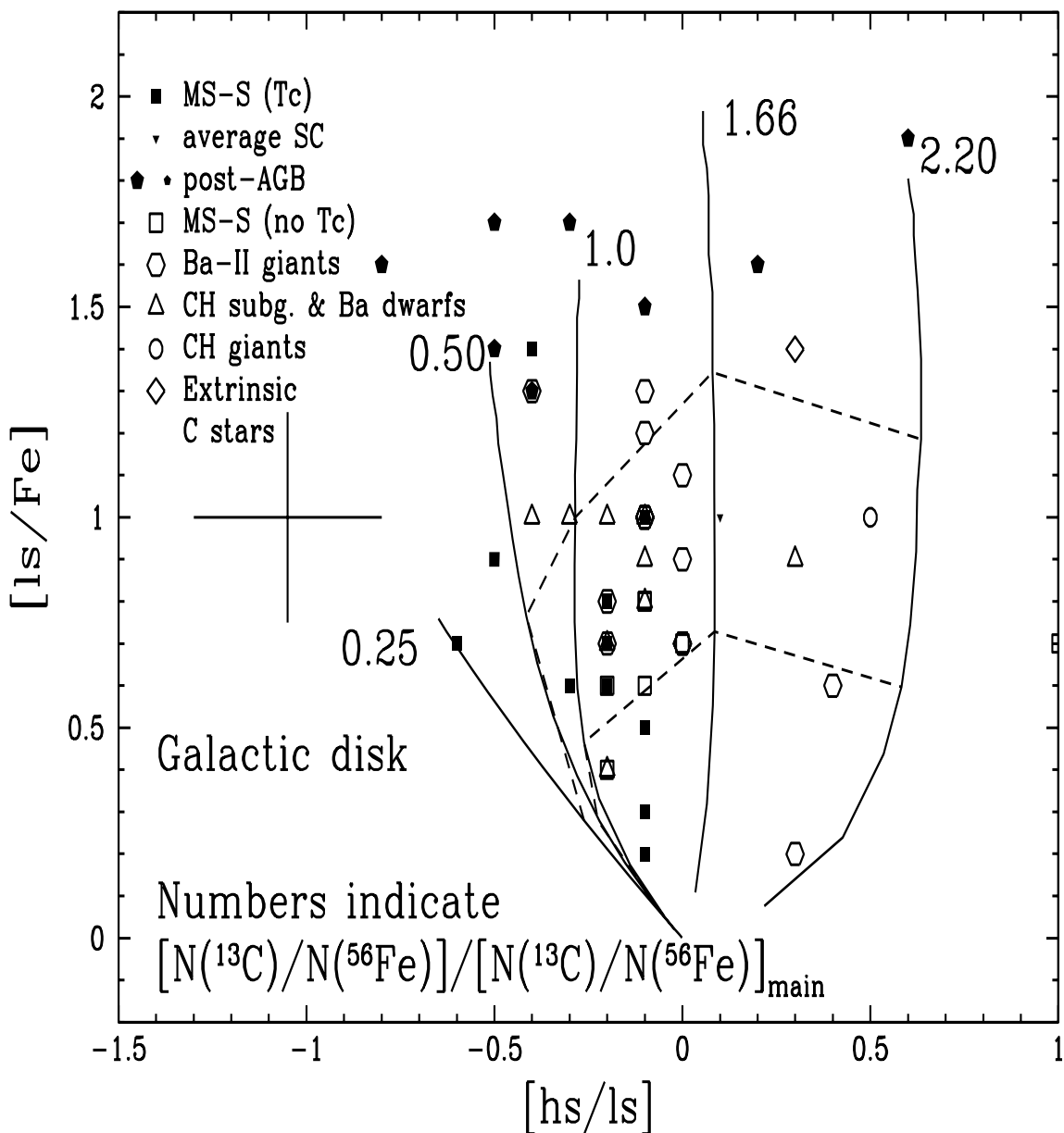


Fig. 10.— The observed trend of the light  $s$ -element abundances  $[ls/Fe]$  versus  $[hs/ls]$ , for Galactic disk intrinsic and extrinsic AGB stars. Continuous curves refer to envelope models with different  $s$ -process efficiency, as monitored by the  $N(^{13}\text{C})/N(^{56}\text{Fe})$  ratio (here normalized to the case that fits the main component in the solar system). Dashed lines connect the points corresponding to the 4th and 8th dredge up episode, to make clear how the stars distribute along the TP-AGB evolutionary sequence.

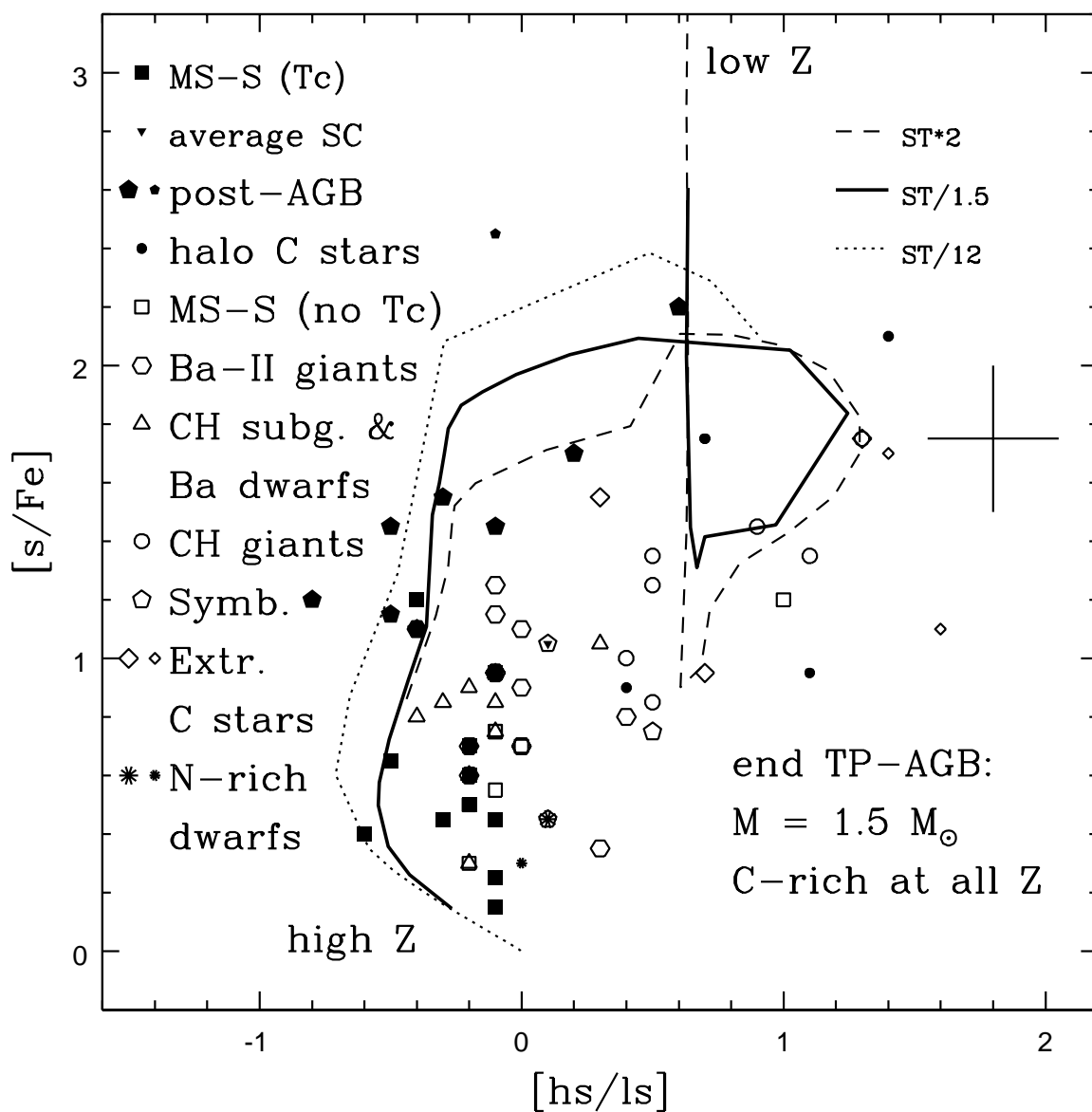


Fig. 11.— The average  $s$ -process enrichment  $[s/Fe]$  as a function of the  $[hs/ls]$  abundance ratio, for the various classes of stars studied. The post-AGB supergiants lay in the region of the maximum  $s$  enrichment, as expected. Curves refer to  $1.5 M_{\odot}$  AGB model stars. They reflect the enrichment of  $s$  elements for different metallicities at the very end of the TP-AGB phase. The regions where the highest and lowest metallicities explored lie are indicated.

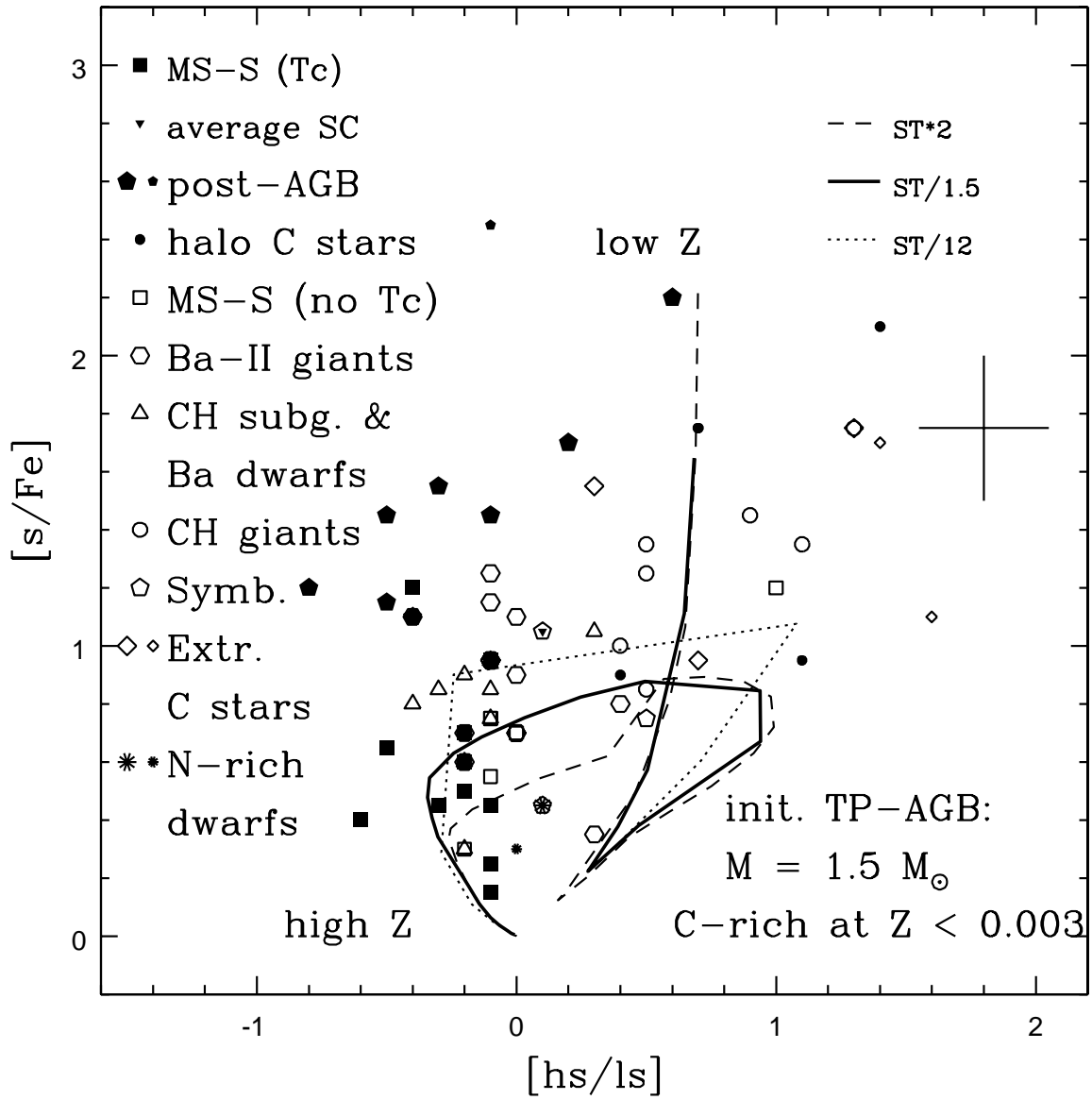


Fig. 12.— Same as Figure 11, but for a much larger dilution with an unprocessed envelope, as obtained at an initial phase of TP-AGB evolution, after only 4 TDU episodes.

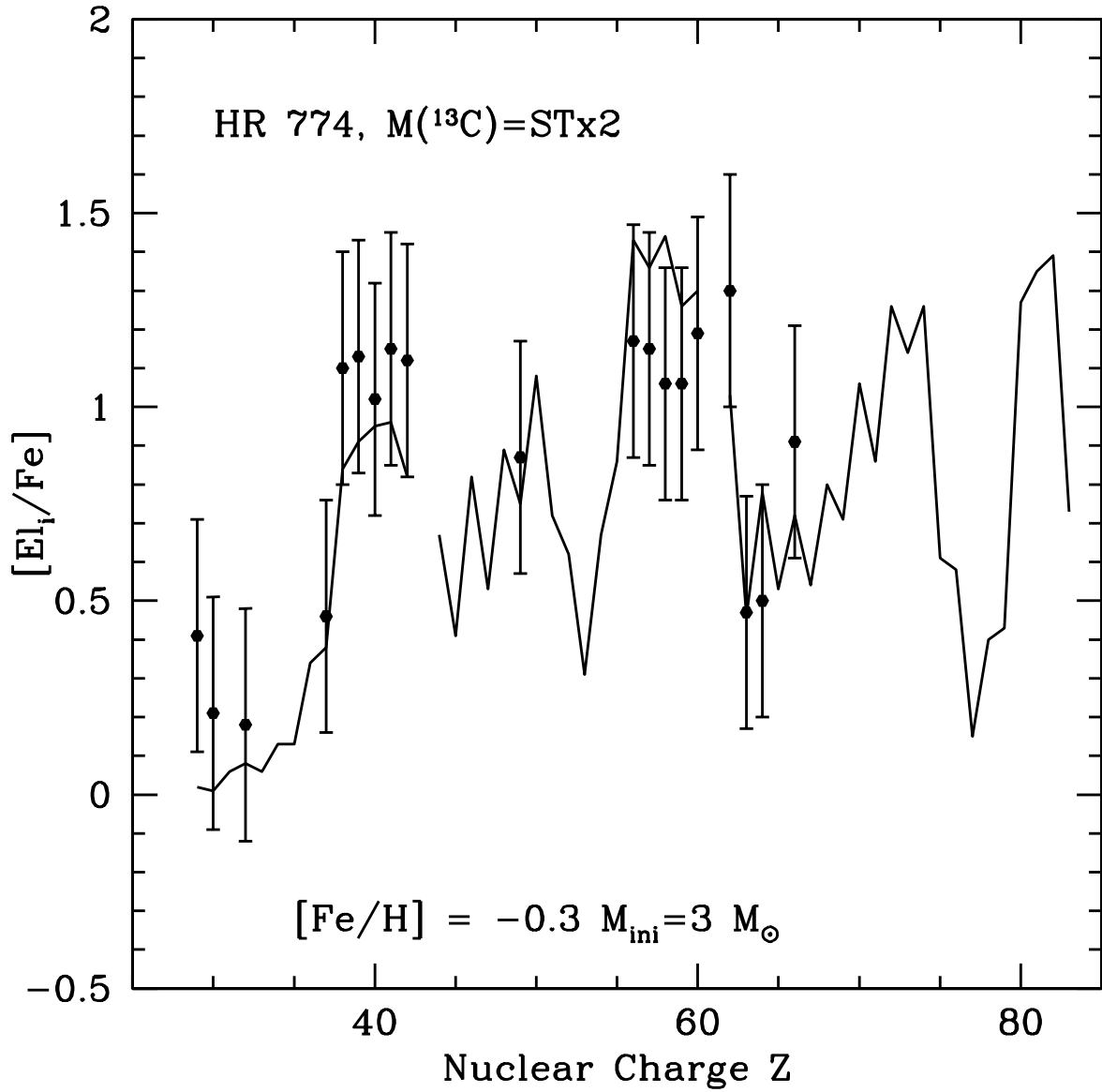


Fig. 13.— A detailed reproduction of observed abundances for the classical Ba II giant HR 774. Observations are from Smith (1984) and Tomkin & Lambert (1983), as compiled in Paper II. See text for details.

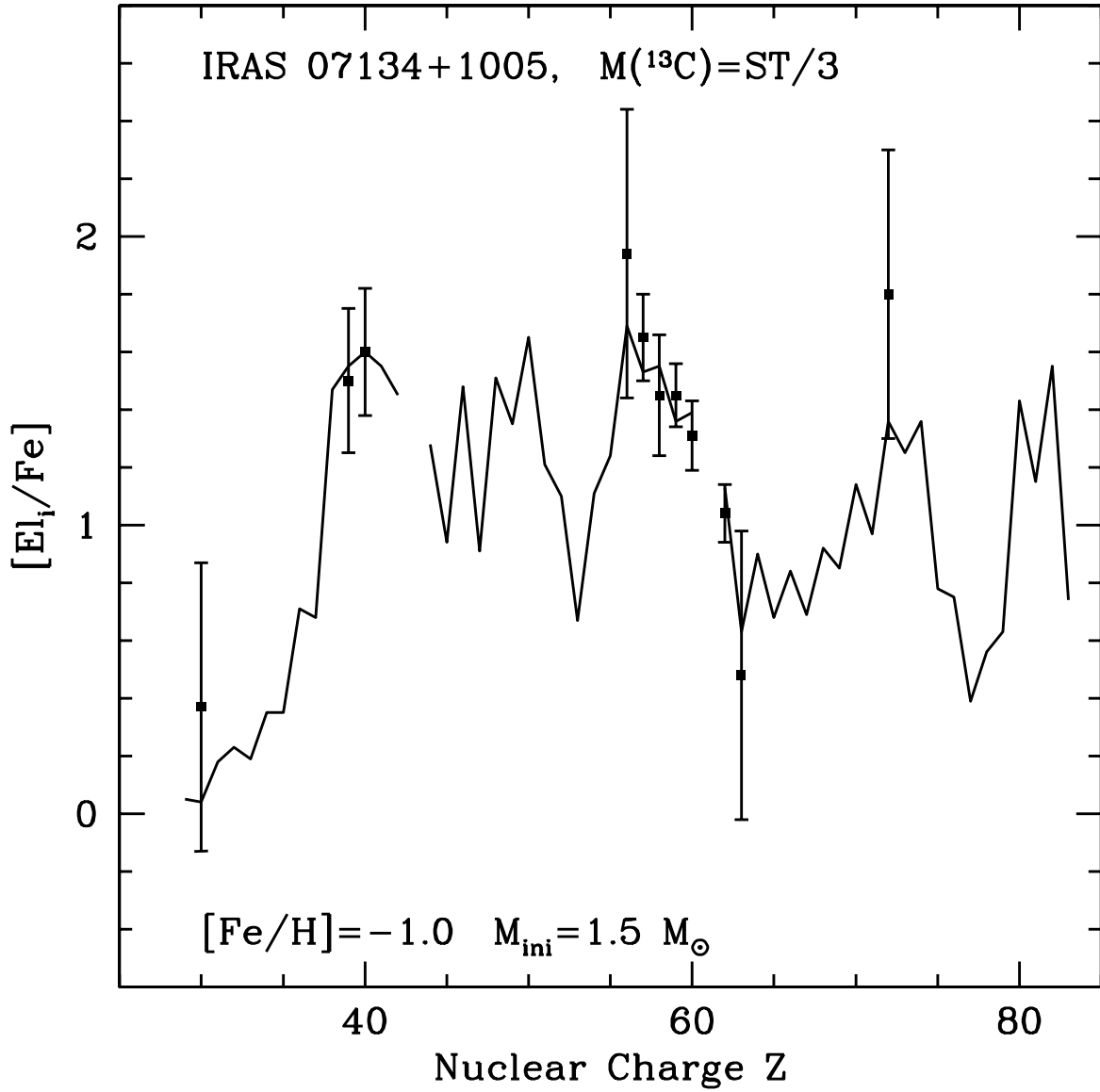


Fig. 14.— A detailed reproduction of observed abundances for the post-AGB supergiant IRAS 07134+1005. Observations are from Van Winckel & Reyniers (2000). See text for details.

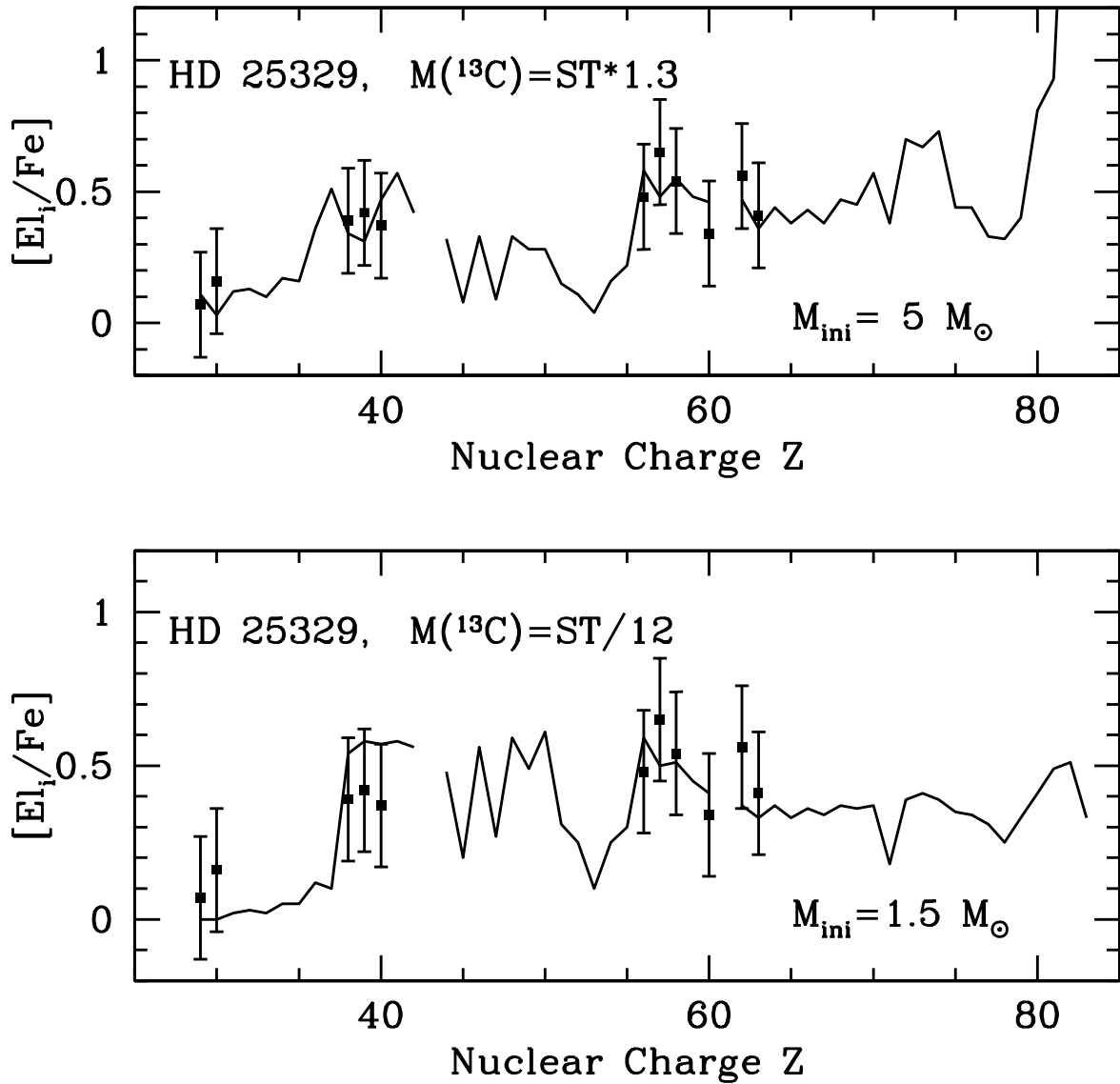


Fig. 15.— Two attempts at reproducing the observed data for the population II s-enriched dwarf HD 25329, performed with a LMS and a IMS model. Observations are from Beveridge & Sneden (1994). See text for details.

TABLE 1

TP	zone	M(TP) ( $M_{\odot}$ )	$\delta(\tau)$ ( $\text{mbarn}^{-1}$ )	$^{94}\text{Zr}/^{94}\text{Zr}_{\odot}$	$^{138}\text{Ba}/^{138}\text{Ba}_{\odot}$	$^{208}\text{Pb}/^{208}\text{Pb}_{\odot}$
1	layer 1		0.194	266	7.5	3.8
	layer 2		0.233	1240	15.9	4.7
	$^{13}\text{C}$ pocket end 2 <sup>nd</sup> TP	0.019		973 39	13.6 1.5	4.4 1.1
2	layer 1		0.189	1020	329	4.1
	layer 2		0.229	1920	684	5.4
	$^{13}\text{C}$ pocket end 3 <sup>rd</sup> TP	0.018		1670 91	587 25	5.0 1.2
5	layer 1		0.183	1680	730	19
	layer 2		0.222	2540	1330	34
	$^{13}\text{C}$ pocket end 6 <sup>th</sup> TP	0.016		2300 175	1170 82	30 2.7
10	layer 1		0.177	1880	986	68
	layer 2		0.216	2720	1630	107
	$^{13}\text{C}$ pocket end 11 <sup>th</sup> TP	0.013		2490 236	1450 145	96 10
15	layer 1		0.168	1960	1030	81
	layer 2		0.207	2770	1670	123
	$^{13}\text{C}$ pocket end 16 <sup>th</sup> TP	0.011		2550 273	1490 174	112 14
20	layer 1		0.161	2160	1170	99
	layer 2		0.199	2960	1830	149
	$^{13}\text{C}$ pocket end 21 <sup>th</sup> TP	0.0093		2740 351	1650 231	136 20

TABLE 2a. INTRINSIC GALACTIC-DISK AGB STARS

STAR	ALIAS	[Fe/H]	[ls/Fe]	[hs/Fe]	[hs/ls]	Type	Ref.
HD 30959	$\alpha^1$ Ori	−0.11	0.9	0.4	−0.5	MS/S (Tc)	(1)
HD 58521	Y Lyn	−0.18	0.7	0.5	−0.2	idem	(2)
HD 64332	NQ Pup	−0.25	0.6	0.4	−0.2	idem	(2)
HD 78712	HR 3639	−0.17	0.8	0.6	−0.2	idem	(3)
HD 106198	HR 4647	−0.04	0.2	0.1	−0.1	idem	(2)
HD 163990	HR 6702	−0.09	0.7	0.1	−0.6	idem	(1)
HD 172804	V679 Oph	−0.06	1.0	0.9	−0.1	idem	(2)
HD 199799	V2141 Cyg	0.17	0.6	0.3	−0.3	idem	(2)
HD 200527	HR 8062	0.06	0.3	0.2	−0.1	idem	(3)
HD 216672	HR 8714	−0.07	0.5	0.4	−0.1	idem	(3)
BD +48°1187	TV Aur	0.07	1.4	1.0	−0.4	idem	(2)
HD 144578	RR Her	0.20	1.0	1.5	0.5	SC	(4)
HD 198164	CY Cyg	0.20	0.8	0.7	−0.1	idem	(4)
HD 286340	GP Ori	0.00	1.4	1.2	−0.2	idem	(4)
CD −52°5798	AM Cen	0.30	0.9	1.0	0.1	idem	(4)
Average SC	(see text)	0.18	1.0	1.1	0.1	—	—
HD 56126	IRAS 07134+1005	−1.00	1.5	1.4	−0.1	post AGB	(5)
HD 187885	IRAS 19500−1709	−0.60	1.4	0.9	−0.5	idem	(5)
HD 235858	IRAS 22272+5435	−0.49	2.4	2.5	−0.1	idem	(6)
IRAS 04296+3429	GLMP 74	−0.60	1.7	1.4	−0.3	idem	(5)
IRAS 05341+0852	GLMP 106	−0.80	1.9	2.5	0.6	idem	(5)
IRAS 07430+1115	GLMP 192	−0.46	1.7	1.2	−0.5	idem	(7)
IRAS 22223+4327	GLMP 1058	−0.30	1.3	0.9	−0.4	idem	(5)
IRAS 23304+6147	GLMP 1078	−0.80	1.6	1.8	0.2	idem	(5)
IRAS Z02229+6208	—	−0.45	1.6	0.8	−0.8	idem	(7)



**TABLE 2b.** INTRINSIC GALACTIC-HALO AGB STARS

STAR	ALIAS	[Fe/H]	[ls/Fe]	[hs/Fe]	[hs/ls]	Type	Ref.
HD 25408	UV Cam	−0.82	0.7	1.1	0.4	Halo C star	(8)
HD 59643	NQ Gem	−0.70	1.4	2.1	0.7	idem	(8)
HD 187216	SAO 3243	−2.50	1.4	2.8	1.4	idem	(9)
HD 189711	SAO 125356	−1.15	1.4	2.1	0.7	idem	(8)
HD 197604	CGCS 4947	−0.90	0.4	1.5	1.1	idem	(8)

TABLE 2c. EXTRINSIC GALACTIC-DISK AGB STARS

STAR	ALIAS	[Fe/H]	[ls/Fe]	[hs/Fe]	[hs/ls]	Type	Ref.
HD 7531	HR 363	−0.13	0.8	0.7	−0.1	MS-S no Tc	(1)
HD 22649	HR 1105	−0.07	0.8	0.7	−0.1	idem	(3)
HD 35155	IRAS 05199−0842	−0.53	0.7	1.7	1.0	idem	(2)
HD 49368	IRAS 06457+0535	−0.21	0.7	0.7	0.0	idem	(2)
HD 119667	BD −02°3726	−0.17	0.6	0.5	−0.1	idem	(2)
HD 147923	BD +57°1671	−0.01	0.4	0.2	−0.2	idem	(2)
HD 151011	BD −18°4320	0.04	0.6	0.4	−0.2	idem	(2)
HD 16458	HR 774	−0.43	1.3	0.9	−0.4	Ba II giant	(10)
HD 44896	SAO 196752	−0.25	1.0	0.9	−0.1	idem	(11)
HD 46407	HR 2392	−0.42	1.2	1.1	−0.1	idem	(12)
HD 60197	SAO 173956	−0.05	0.7	0.7	0.0	idem	(11)
HD 104979	o Vir	−0.47	0.6	1.0	0.4	idem	(13)
HD 116713	HR 5058	−0.29	1.1	1.1	0.0	idem	(12)
HD 121447	IT Vir	0.05	0.7	0.7	0.0	idem	(11)
HD 139195	HR 5802	−0.24	0.7	0.5	−0.2	idem	(13)
HD 178717	SAO 104535	−0.18	0.9	0.9	0.0	idem	(11)
HD 204075	ζ Cap	−0.11	1.0	0.9	−0.1	idem	(14,15)
DM −64°4333	MFU 149	0.05	0.8	0.6	−0.2	idem	(11)
NGC 2420-D	—	−0.45	0.2	0.5	0.3	idem	(16)
NGC 2420-X	—	−0.58	1.3	1.2	−0.1	idem	(16)
HD 4395	SAO 147438	−0.33	0.7	0.5	−0.2	CH subgiant	(17)
HD 11377	SAO 148062	−0.05	0.4	0.2	−0.2	idem	(17)
HD 88446	SAO 98999	−0.36	0.9	0.8	−0.1	idem	(17)
HD 89948	SAO 178741	−0.27	1.0	0.7	−0.3	idem	(17)
HD 125079	SAO 139848	−0.16	1.0	0.8	−0.2	idem	(17)
HD 182274	SAO 104781	−0.18	0.8	0.7	−0.1	idem	(17)
HD 204613	SAO 33445	−0.35	1.0	0.6	−0.4	idem	(17)
HD 216219	SAO 108214	−0.32	1.0	0.9	−0.1	idem	(17)
HD 219116	SAO 165564	−0.34	0.9	1.2	0.3	idem	(17)
HD 26	SAO 109003	−0.40	1.0	1.5	0.5	CH giant	(18)
BD +75°348	SAO 6630	−0.80	1.4	1.7	0.3	Extr. C giant	(19)

TABLE 2d. EXTRINSIC GALACTIC-HALO AGB STARS

STAR	ALIAS	[Fe/H]	[ls/Fe]	[hs/Fe]	[hs/ls]	Type	Reference
HD 187861	CGCS 4524	−1.65	1.0	1.9	0.9	CH giant	(18, 20)
HD 198269	SAO 106516	−1.40	0.8	1.2	0.4	idem	(18)
HD 201626	SAO 89499	−1.30	1.1	1.6	0.5	idem	(18)
HD 209621	HP Peg	−0.90	1.1	2.4	1.3	idem	(18)
HD 224959	BD −03°5751	−1.60	0.8	1.9	1.1	idem	(18)
CD −38°2151	SAO 196068	−1.40	0.6	1.1	0.5	idem	(18)
BD +67°922	AG Dra	−1.30	0.5	1.0	0.5	Yellow Symb.	(21)
BD −21°3873	IV Vir	−1.32	0.4	0.5	0.1	idem	(22)
He 2-467	—	−1.11	1.0	1.1	0.1	idem	(23)
HD 196944	SAO 144688	−2.45	0.6	1.3	0.7	C-rich giant	(24)
LP 625−44	—	−2.71	1.1	2.4	1.3	C-rich subgiant	(25)
CS 22898−027	—	−2.35	1.0	2.4	1.4	idem	(26, 27)
LP 706−7	—	−2.74	0.3	1.9	1.6	idem	(28)
HD 74000	SAO 154538	−2.08	0.3	0.3	0.0	N-rich dwarf	(28)
HD 25329	SAO 56928	−1.84	0.4	0.5	0.1	idem	(29)

(1) Smith & Lambert (1985); (2) Smith & Lambert (1990); (3) Smith & Lambert (1986); (4) Abia & Wallerstein (1998); (5) Van Winckel & Reyniers (2000); (6) Začs et al. (1995); (7) Reddy et al. (1999); (8) Kipper et al. (1996); (9) Kipper & Jørgensen (1994); (10) Tomkin & Lambert (1983); (11) Smith (1984); (12) Kovács (1985); (13) Tomkin & Lambert (1986); (14) Smith & Lambert (1984); (15) Tech (1971); (16) Smith & Suntzeff (1987); (17) Smith et al. (1993). (18) Vanture (1992); (19) Začs et al. (2000); (20) Vanture (2000); (21) Smith et al (1996); (22) Smith et al. (1997); (23) Pereira et al. (1998); (24) Začs et al. (1998); (25) Aoki et al. (2000); (26) McWilliam et al. (1995); (27) McWilliam (1998); (28) Norris et al. (1997); (29) Beveridge & Sneden (1994)